iScience

CellPress

Article

Mutant and Wild-Type Tumor Suppressor p53 Induces p300 Autoacetylation

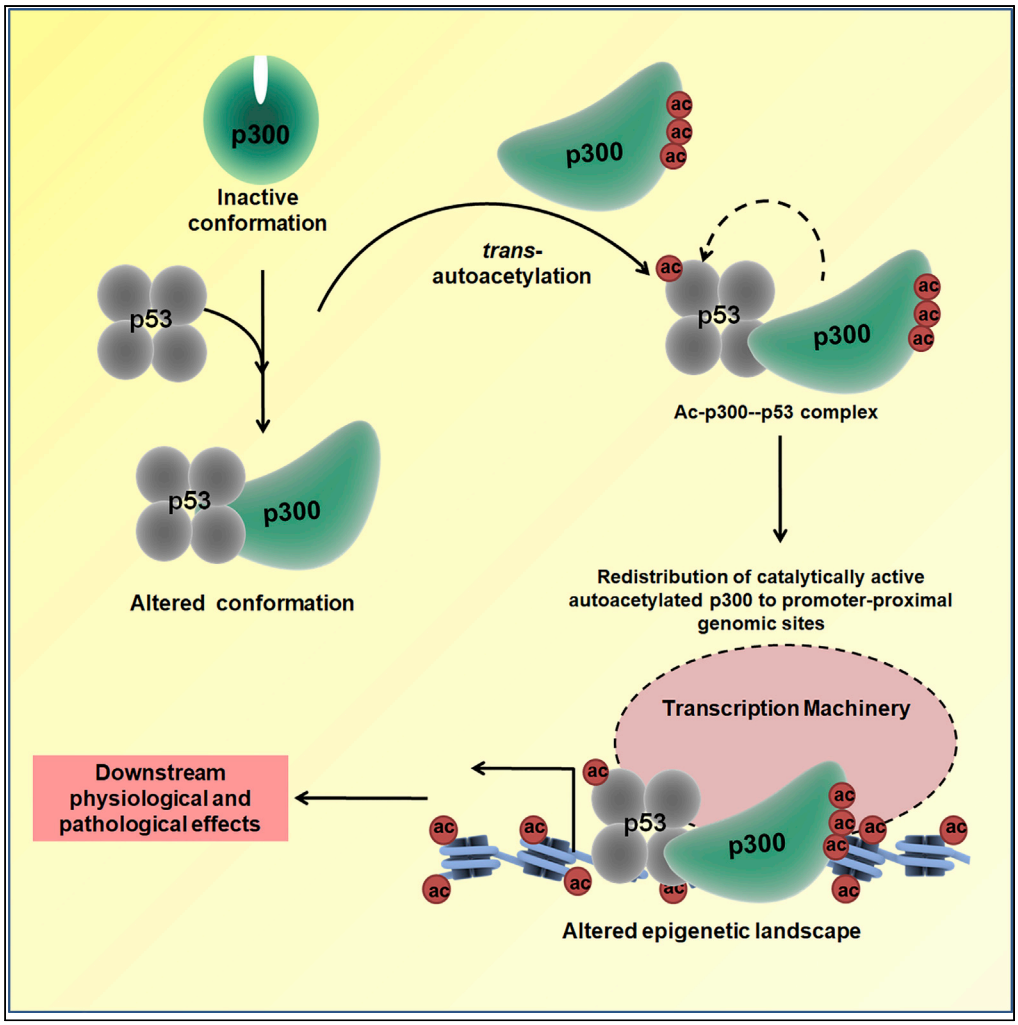

Stephanie Kaypee, Smitha Asoka Sahadevan, Shilpa Patil, Piya Ghosh, Neeladri Sekhar Roy, Siddhartha Roy, Tapas K. Kundu

tapas@jncasr.ac.in

HIGHLIGHTS

Wild-type and mutant p53 are potent inducers of p300 autoacetylation

p53 activates p300 catalytic activity by altering its structural conformation

Induction of p300 autoacetylation possibly enhances p53-targeted gene expression

Mutant-p53-induced p300 autoacetylation could be critical for tumorigenicity

Kaypee et al., iScience 4, 260–272
June 29, 2018
https://doi.org/10.1016/j.isci.2018.06.002

iScience

CellPress

Article

Mutant and Wild-Type Tumor Suppressor p53 Induces p300 Autoacetylation

Stephanie Kaypee,[1] Smitha Asoka Sahadevan,[1] Shilpa Patil,[1,3] Piya Ghosh,[2] Neeladri Sekhar Roy,[2,4] Siddhartha Roy,[2] and Tapas K. Kundu[1,5,*]

SUMMARY

The transcriptional co-activator p300 is essential for p53 transactivation, although its precise role remains unclear. We report that p53 activates the acetyltransferase activity of p300 through the enhancement of p300 autoacetylation. Autoacetylated p300 accumulates near the transcription start sites accompanied by a similar enrichment of activating histone marks near those sites. Abrogation of p53-p300 interaction by a site-directed peptide inhibitor abolished p300-mediated histone acetylation, suggesting a crucial role played by the activation in p53-mediated gene regulation. Gain-of-function mutant p53, known to impart aggressive proliferative properties in tumor cells, also activates p300 autoacetylation. The same peptide abolished many of the gain-of-function properties of mutant p53 as well. Reversal of gain-of-function properties of mutant p53 suggests that molecules targeting the p53-p300 interface may be good candidates for anti-tumor drugs.

INTRODUCTION

Organismic complexity scales with the intricacies and sophistication of gene regulation. How this intricate regulation is achieved, however, is not fully understood. Specificity, both spatial and temporal, is at the heart of this extraordinarily elaborate and complex regulatory process (Levine and Tjian, 2003). Protein-protein interactions among multiple transcription factors bound to adjacent sequences, DNA-mediated cooperativity, and other factors have been found to enhance site selectivity and to initiate the assembly of multi-protein regulatory complexes. After assembly the regulatory complex initiates the recruitment of co-activators, chromatin modifiers, and other factors, thereby increasing chromatin accessibility and the initiation of RNA synthesis (Dulac, 2010; Schneider and Grosschedl, 2007). It is not known whether any steps beyond the assembly of regulatory complexes influence the spatial and temporal specificity of gene regulation.

p300 (KAT3B) is a transcriptional co-activator with intrinsic acetyltransferase activity. Being a large adaptor protein, p300 bridges the basal transcription machinery to DNA sequence-specific transcription factors (Chan and La Thangue, 2001; Ogryzko et al., 1996). By virtue of its structural plasticity, p300 can interact with the intrinsically disordered transactivation domains of a vast array of transcription factors, thereby functioning as a nodal integrator of signals terminating in the regulation of transcription (Bedford et al., 2010; Dyson and Wright, 2016; Lee et al., 1998; Perissi et al., 1999). Therefore, its recruitment via the interaction with sequence-specific transcription factors can regulate transcription from the chromatin template (Kundu et al., 2000). This protein is often recruited to assembled regulatory complexes, where it acetylates histone tails in the vicinity. In this way, p300 promotes localized chromatin accessibility and, subsequently, selective transcriptional initiation (Vo and Goodman, 2001).

The basal catalytic activity of p300 is enhanced by *trans*-autoacetylation of its lysine-rich regulatory loop (Thompson et al., 2004). It had been proposed that, in the absence of acetylation, the positively charged lysine-rich auto-inhibitory loop folds back onto the enzyme active site, thus hindering optimal substrate-enzyme interaction. Since p300 is involved in diverse physiological roles, the precise regulation of its function is essential. It has been demonstrated that some factors affect the levels of p300 autoacetylation in the cell. Intriguingly, these factors have distinct cellular functions and induce p300 autoacetylation under different cellular contexts. The Anaphase Promoting Complex/Cyclosome (APC/C) subunits APC5 and APC7 are capable of enhancing p300 autoacetylation, which is required for proper cell cycle progression (Turnell et al., 2005). Similarly, the transcription factor MAML1 has been shown to increase the levels of p300 autoacetylation, thereby inducing the transcription of Notch pathway genes (Hansson et al., 2009). During cellular stress, GAPDH associates with the E3 ligase Siah1 and shuttles to the nucleus, where it

[1]Transcription and Disease Laboratory, Molecular Biology and Genetics Unit, Jawaharlal Nehru Centre for Advanced Scientific Research, Bangalore 560064, India

[2]Department of Biophysics, Bose Institute, Kolkata 700054, India

[3]Present Address: Department of Gastroenterology and GI oncology, University Medical Center, Goettingen 37075, Germany

[4]Present Address: Laboratory of Cellular and Molecular Biology, National Cancer Institute, National Institutes of Health, Bethesda, MD 20892, USA

[5]Lead Contact

*Correspondence: tapas@jncasr.ac.in

https://doi.org/10.1016/j.isci.2018.06.002

enhances p300 autoacetylation, which in turn activates the p53-mediated apoptotic pathway (Sen et al., 2008). p300 autoacetylation is negatively regulated by the class III lysine deacetylase SIRT2, and as expected, the suppression of p300 autoacetylation leads to the reduction of its enzymatic activity (Black et al., 2008). We have previously reported the presence of global histone hyperacetylation in oral cancer. Mechanistically, this abnormality is a consequence of enhanced p300 autoacetylation, which is induced by NPM1 and nuclear GAPDH in a nitric oxide (NO) signaling-dependent manner. Ac-p300 may be the driving force that causes alterations in the epigenetic landscape and, consequently, the global deregulation of transcription that is required for oral carcinogenesis (Arif et al., 2010). Thus, modulation of p300 autoacetylation may be a key factor in regulating cellular responses.

p300 is a co-activator of the tumor suppressor p53 and acetylates it on several lysine residues, mainly on its C-terminal domain (Gu and Roeder, 1997; Lill et al., 1997). Studies have attributed the enhancement of DNA sequence-specific binding ability of p53 to the p300-mediated acetylation, whereas contradictory findings have shown that p53 C-terminal acetylation may not have a profound effect on its promoter binding (Barlev et al., 2001; Espinosa and Emerson, 2001). Nevertheless, accumulation of acetylated p53 has been observed during cellular stresses (Reed and Quelle, 2014; Sakaguchi et al., 1998) and p53 acetylation has been studied extensively with respect to cell cycle arrest, apoptosis, senescence, and ferroptosis (Bieging et al., 2014; Jiang et al., 2015). Studies using the acetylation-defective mutants of p53 have shown that the acetylation of p53 is not required for its DNA binding, rather it is crucial for the recruitment of co-activators such as p300, which are essential for p53 transactivation function (Barlev et al., 2001), thereby reiterating the fact that the interaction between p300 and p53 is functionally important. p53 interacts with p300 in its tetrameric conformation, through its bipartite transactivation domain AD1 and AD2, whereas p300 interacts through several domains, namely, TAZ1, KIX, TAZ2, and IBiD (Krois et al., 2016; Teufel et al., 2007). Intriguingly, numerous factors such as E1A, DDX24, WTX, MYBB1A, and Skp2, can regulate p53 tumor suppressive functions *in vivo* by dictating its association with p300, thereby proving that the p300-p53 axis is an important cell fate determinant in stress responses (Kim et al., 2012; Kitagawa et al., 2008; Kumazawa et al., 2011; Lill et al., 1997; Shi et al., 2016; Vasudevarao et al., 2014). The p53 gene acquires several mutations that abolish its tumor suppressive functions and confer oncogenic gain-of-function (GOF) properties that contribute to tumorigenesis. Approximately 97% of the missense mutations map to the DNA-binding domain (DBD), of which a small number occur in high frequency in cancers (Freed-Pastor and Prives, 2012). GOF p53 mutants induce aberrant transactivation in cancers through the recruitment of p300, but the effect of mutant p53 on p300 catalytic activity is yet unknown. In the present study, we addressed the mechanism of factor-induced p300 autoacetylation and its importance in p53-dependent gene regulation.

We found that the master tumor suppressor protein p53 specifically induces p300 autoacetylation. Comparison of the genomic distribution of ac-p300 and p300 before and after stimulation by p53 indicates that ac-p300 is specifically and uniquely present around transcription start sites (TSS) of p53-regulated genes. This study establishes the mechanism of p53-mediated induction of p300 autoacetylation and its chromatin recruitment at transcriptional regulatory elements. Our data indicate that GOF mutant p53 may execute its downstream oncogenic functions through the modulation of p300/CBP autoacetylation and function. The implications of these observations are further explored.

RESULTS

p53 Directly Modulates p300 Autoacetylation and Acetyltransferase Activity

To explore whether p53 has an effect on the acetyltransferase activity of p300, an *in vitro* acetyltransferase assay was designed to detect the effect of p53 on the levels of p300 autoacetylation. p53 specifically induced the autoacetylation of 20 nM p300 in a concentration-dependent manner (ranging from 40 to 160 nM p53 monomers) but exhibited a negligible effect on the autoacetylation of the other two classes of lysine acetyltransferases (KATs), PCAF, and Tip60 (Figure 1A). An approximately 4.5-fold enhancement of p300 autoacetylation was observed in the presence of 160 nM p53 (2:1 ratio of p53 tetramers to p300). Because p53 forms a stable tetramer and may possibly interact with p300 as a tetramer (Teufel et al., 2007), a significant degree of p300 autoacetylation was reached only when p53 was present in a 1:1 ratio of tetrameric p53 to p300. At a suboptimal concentration (40 nM) of p53 (tetrameric p53 to p300 ratio of 0.5:1), a negligible increase in the autoacetylation was observed (Figure S1A). Moreover, p53 is a substrate of most major nuclear KATs, including p300/CBP (Gu and Roeder, 1997), PCAF (KAT2B) (Liu et al., 1999), TIP60 (KAT5) (Sykes et al., 2006; Tang et al., 2006), MOZ (KAT6A) (Rokudai et al., 2013), and MOF (KAT8) (Sykes et al., 2006). Therefore, the specificity exhibited by p53 toward the enhancement of p300

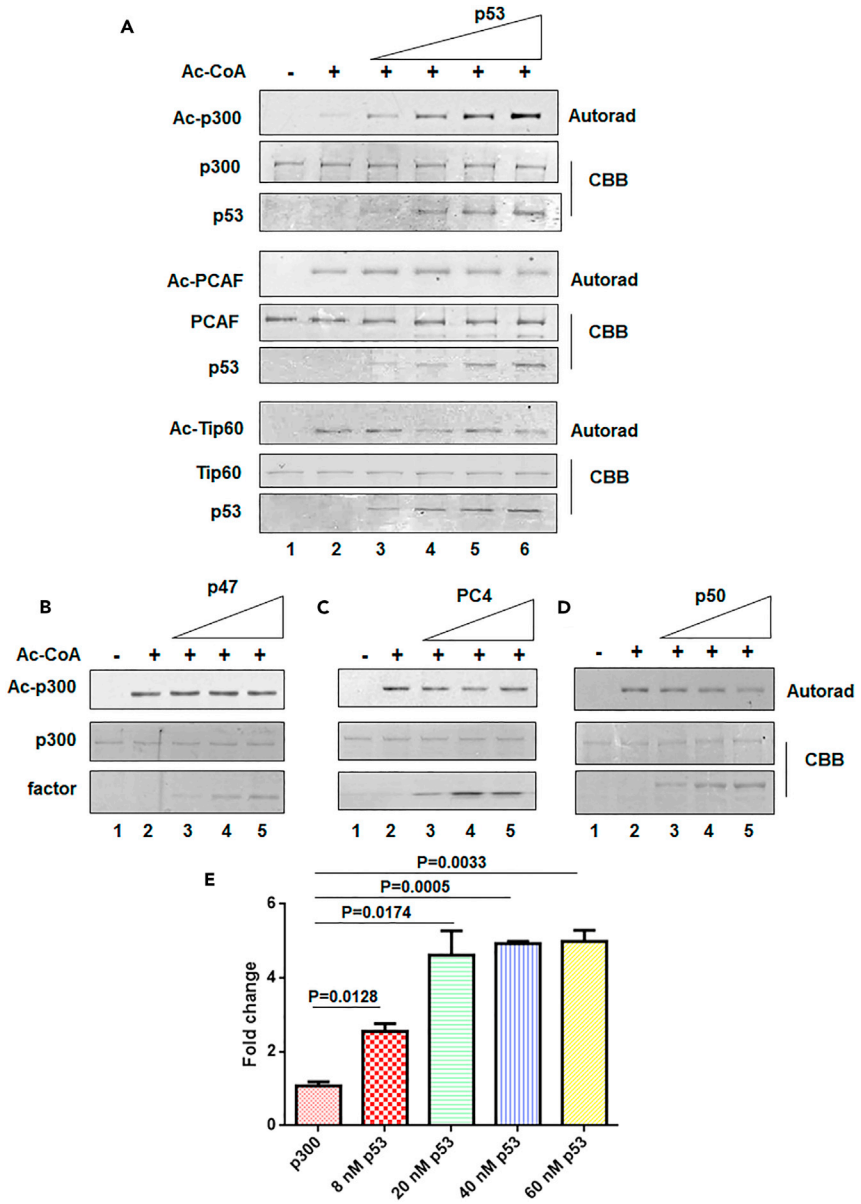

Figure 1. The Tumor Suppressor p53 Enhances p300 Autoacetylation

(A) An *in vitro* acetyltransferase assay was performed to determine the levels of autoacetylation of different lysine acetyltransferases (KATs) in the presence of 40, 80, 120, and 160 nM of recombinant wild-type p53 (Lanes 3-6), respectively. The autoradiograms indicate the levels of p300, PCAF, and Tip60 autoacetylation, respectively, whereas the Coomassie Brilliant Blue (CBB)-stained protein panels show the loading control. (See Figure S1A for densitometric quantification).

(B–D) An *in vitro* acetyltransferase assay was performed to determine the levels of p300 autoacetylation in the presence of different p300 substrates (B) p47, (C) PC4, and (D) p50. 20 nM p300 and 50, 100, and 150 nM of each protein factor were used.

(E) Enhancement of p300 catalytic activity in the presence of increasing concentrations of wild-type p53 as indicated was determined by filter-binding histone acetyltransferase assay, using recombinant histone H3 as substrate. The mean fold change was plotted ±SD; statistical analysis was performed using unpaired two-tailed Student's t test.

autoacetylation, with no effect seen for PCAF and Tip60, led us to conclude that p53 is not merely a substrate of p300 but a regulator of the intrinsic enzymatic activity of p300. This specific role of p53 was investigated further. Three different substrates of p300, p47 (N-terminal truncated [Δ40p53] isoform of p53, incapable of binding to p300), Positive Coactivator 4 [PC4], and p50 (a subunit of nuclear factor κB), were also

tested and found not to effectively induce p300 autoacetylation (Figures 1B–1D). To investigate the effect of the p53-mediated induction of p300 autoacetylation, we performed an *in vitro* histone acetyltransferase assay using recombinant histones as the substrate. In agreement with the results of the autoacetylation assay, we observed an approximately 3-fold increase in p300 histone acetyltransferase activity at a p300:p53 molar ratio of 1:2. Notably, we observed an approximately 4.5-fold increase in p300 activity in the presence of p53, thus suggesting that p53 positively modulates p300 KAT activity through the induction of autoacetylation. Further increase in the p53 concentration did not affect the HAT activity beyond 4.5-fold (Figure 1E). The *in vitro* p53-mediated induction of p300 autoacetylation was further verified in the cellular context. Endogenous p53 levels were stabilized in HepG2 cells by using the small molecule inhibitor of the MDM2-p53 interaction, Nutlin-3a. The stabilization of p53 after Nutlin-3a treatment appeared to positively regulate the levels of p300 autoacetylation in the cells in comparison with cells treated or not treated with DMSO (Figure 2A). Furthermore, the fluorescence intensity due to p300 autoacetylation was significantly ($p < 0.001$) enhanced in HepG2 cells treated with Nutlin-3a expressing wild-type p53 (Figure 2B). We expected that hyper-autoacetylated p300 would induce p300-specific histone acetylation in cells. To address this possibility, histone acetylation at H3K9 and H3K14 were investigated in the presence and absence of Nutlin-3a (Figure 2C). It has been previously demonstrated that p53 acetylation and histone acetylation increase after Nutlin-3a treatment (Haaland et al., 2014). Therefore, to test for whether the enhancement in histone acetylation was due to the p53-mediated enhancement of p300 autoacetylation, we treated p53-null H1299 cells with Nutlin-3a and probed for the levels of different histone acetylation marks in treated versus control cells (Figure 2D). Interestingly, we found that the histone acetylation levels did not show any appreciable alteration in Nutlin-3a-treated H1299 cells, thereby signifying the importance of p53 in the activation of p300 KAT activity. To rule out the possibility that p300 might be transcriptionally regulated by p53 rather than post-translationally modulated, p300 transcript levels were compared between cells treated with Nutlin-3a and DMSO. No change in the levels of *EP300* transcript was observed in the presence of p53 compared with *CDKN1A* (an early p53 target gene) transcripts, thus suggesting that p300 is not regulated by p53 at the transcriptional level (Figure 2E). Collectively, these results established p53 as a *bona fide* inducer of p300 autoacetylation and its acetyltransferase activity. To elucidate the mechanistic details of p53-mediated activation of p300, the importance of the direct interaction between p53 and p300 was investigated. p53 directly contacts p300 through four important residues (L22, W23, W53, F54) in its transactivation domain. Mutations in these residues severely compromise p53 transactivation (Teufel et al., 2007). After DNA damage, p53 is phosphorylated by several kinases, and phosphorylated p53 binds to its co-activator p300 with higher affinity (Lambert et al., 1998; Lee et al., 2010). Interestingly, the higher the number of phosphorylated sites on the p53 N-terminus, the higher its affinity for CBP/p300 (Lee et al., 2009, 2010). A triple-phospho-mimic peptide (S15E, T18E, S20E) comprising the 11^{th} to 30^{th} amino acid residue of the p53 (TAD1 domain) protein along with a cell penetrating sequence and nuclear localization sequence (NLS) was used to obstruct the interaction between p53 and p300 (Polley et al., 2008) (Figure S1B, Table S1). Using a filter-binding assay-based strategy, the importance of the p53-p300 interaction for the activation of p300 was assessed on the basis of the level of p300-mediated histone acetylation (Figure 2F). The peptides and p53 alone did not bind to the p81 phosphocellulose filters; therefore, the measured radioactivity was only from the tritium-labeled acetylated histones bound to the filters. The basal activity of p300 in the absence of any inducer was considered as 100% activity, and the peptides alone did not alter the activity of p300, thus signifying that any change in histone acetylation observed thereafter was a direct consequence of the p300-p53 interaction. In the presence of 4 nM p53, a 3-fold increase in the histone acetylation was observed. The presence of scrambled peptide did not alter the p53-mediated induction of p300 activity, but p53 phosphomimic peptides (3E pep) effectively decreased histone acetylation levels. These results indicated that the p53 phosphomimic peptide effectively interfered with the p53-p300 interaction, thus presumably leading to decreased p300 autoacetylation and activity, as indicated by a significant decrease in histone acetylation levels. The scrambled peptide exhibited a negligible effect on p53-mediated p300 activation, thus ensuring that the decrease observed in the case of the p53 phosphomimic peptide was indeed due to the disruption of the p53-p300 axis and was not a non-specific effect of the peptides (Figure 2F). Furthermore, to ascertain whether these peptides were effective in cells, HepG2 cells were treated with Nutlin-3a to stabilize the levels of p53. The cells were then treated with different concentrations of the p53 phosphomimic peptide, which has cell-penetrating sequences (Figure 2G). The levels of p53 increased after Nutlin-3a treatment, and the peptide treatment did not alter p53 protein levels. Therefore, the p53 peptide did not alter cellular p53 protein levels, and the observed alteration in histone acetylation is a direct consequence of the disruption of p53-p300 interaction. In agreement with the previous observation, H2AK5 acetylation increased on p53 stabilization with

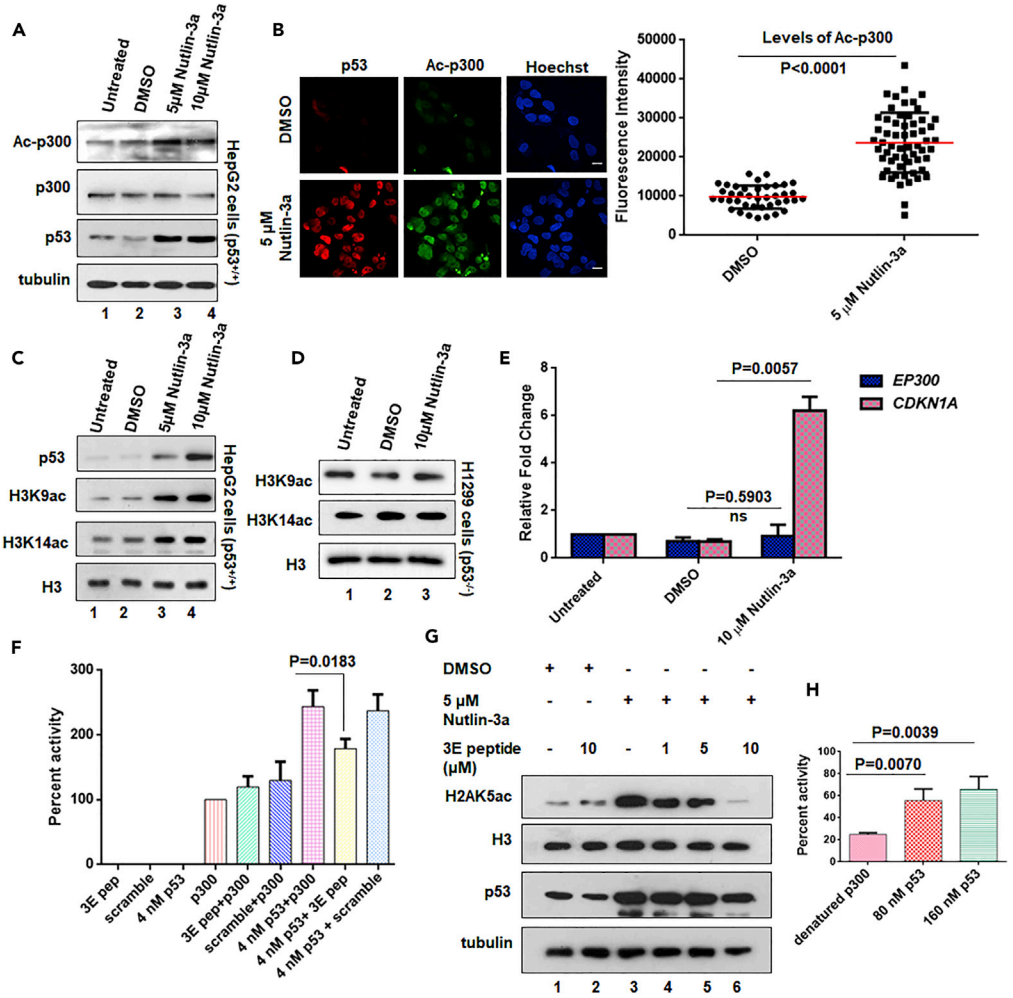

Figure 2. p53 Modulates p300 Autoacetylation and Acetyltransferase Activity in Cells

(A) HepG2 cells were treated with DMSO (vehicle control) or Nutlin-3a as indicated (lane 2–4); levels of Ac-p300, p300, and p53 were analyzed by immunoblotting. Alpha-tubulin levels were considered as the loading control.

(B) HepG2 cells were treated with 5 μM Nutlin-3a for 24 hr, and the levels of Ac-p300 and p53 were assessed by co-immunofluorescence. Fluorescence intensity of Ac-p300 in control cells versus Nutlin-3a-treated cells have been quantified (represented as mean ± SD, unpaired two-tailed Student's t test, n = 50 of three independent experiments). Scale bar, 10 μm.

(C and D) HepG2 cells (C) and H1299 cells (D) were treated with DMSO (vehicle control) or Nutlin-3a as indicated. Histone acetylation levels were analyzed by immunoblotting using H3K9ac and H3K14ac antibodies. Total histone H3 levels were used as the loading control.

(E) The relative transcript levels of *EP300* and *CDKN1A* (p53-responsive gene) were determined by qRT-PCR (mean ± SD). Unpaired two-tailed Student's t test statistical analysis was performed. Actin transcript level was used as the internal control. The relative p300 transcripts do not alter significantly on Nutlin-3a treatment.

(F) Results of filter-binding assay indicate that the p53 phosphomimic N-terminal peptide (3E pep) can effectively reduce the activity of p300 by interfering with its interaction to p53; 4 nM p53 phosphomimic and scrambled peptides were used. (Also see Figure S1B.)

(G) HepG2 cells treated with Nutlin-3a or DMSO, and p53 phosphomimic peptide (3E peptide) as indicated, and the levels of H2AK5ac, H3, p53, and tubulin were probed by immunoblotting. (Also see Figure S1C.)

(H) The rescue of heat-denatured 20 nM p300 activity (activity rescue assay), on addition of wild-type p53, at the indicated concentrations, was determined by the *in vitro* filter-binding assay, using recombinant histone H3 and [^{3}H] acetyl-CoA.

Nutlin-3a (Figures 2G and S1C). After treatment with the interfering peptide, the levels of H2AK5 acetylation gradually decreased in a concentration-dependent manner (Figure 2G), whereas H2AK5ac levels remained unchanged after scrambled peptide treatment (Figure S1C). The direct interaction between p300 and p53 appeared to be crucial for the induction of p300 catalytic activity; therefore, we wanted to

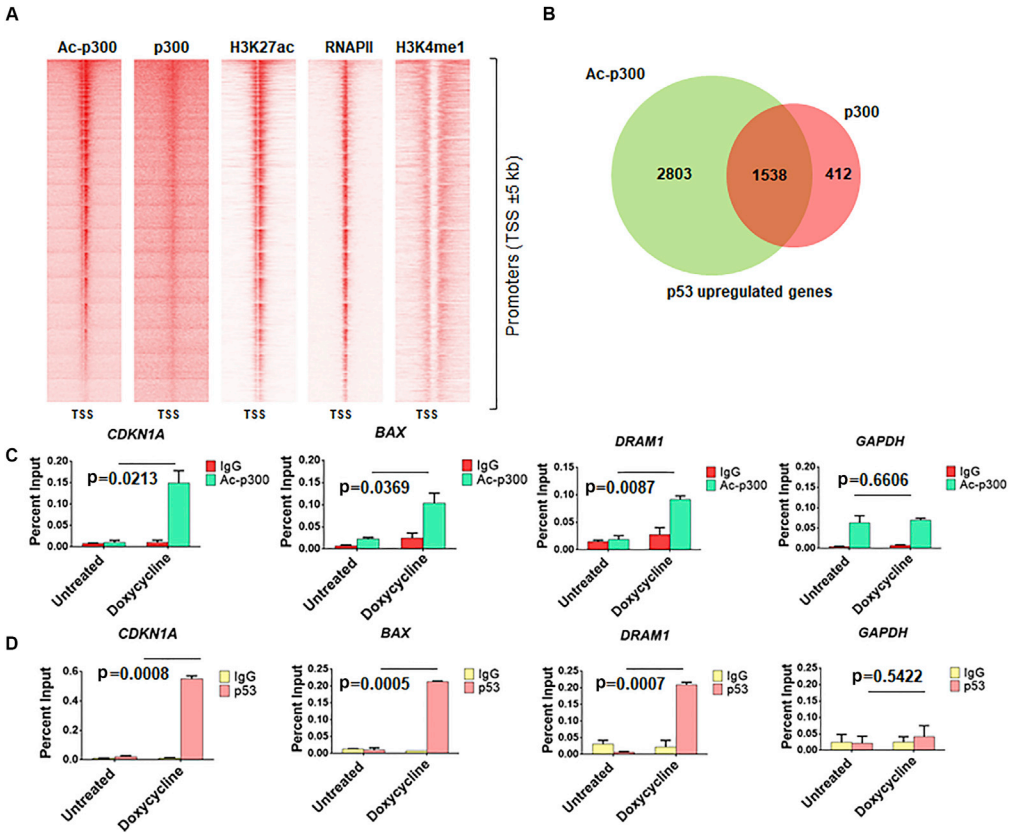

Figure 3. Redistribution of p300 after p53-Mediated Enhancement of p300 Autoacetylation

(A) Heatmaps depicting the enrichment of ac-p300, p300, H3K27ac, RNA Polymerase II (RNAPII), and H3K4me1 at promoters (TSS ±5 kb).

(B) Venn diagram showing the overlap between the up-regulated genes enriched at the promoters with both ac-p300 and p300 and genes unique to each set.

(C and D) ChIP-qPCR to determine the occupancy of (C) p53 and (D) autoacetylated p300 (Ac-p300) at p53-responsive gene promoters. (See Figure S2.)

investigate whether p53 could modulate the structure of p300. Since p300 is a large, intrinsically disordered protein of 300 kDa, it could be a possibility that p53 may act as a molecular chaperone for p300, thereby stabilizing its disordered structure. To address this, we designed an *in vitro* radioactivity-based histone acetyltransferase assay whereby we denatured p300 at 45°C and then incubated the denatured enzyme with p53 at 30°C. The refolding or recovery of p300 activity was scored by its ability to acetylate recombinant histones. Interestingly, we observed a p53 concentration-dependent rescue of p300 activity, suggesting that p53 could possibly act as a molecular chaperone for p300 (Figure 2H). Overall, we observed that p53 is a potent inducer of p300 autoacetylation and enzymatic activity, which may be through the modulation of p300 structure by p53.

Redistribution of Autoacetylated p300 upon p53-Mediated Activation

If the p53-mediated activation of p300 is important for p53-mediated regulation of targeted genes, then it is expected that activated forms should be present in the vicinity of the regulated genes. We have thus attempted to explore the effect of p53 expression on the presence of p300 in different genomic sites. The differential occupancy of ac-p300 and p300 on the promoters of genes that are expressed after p53 stimulation has been investigated. The enrichment patterns indicated a distinct preference of ac-p300 for the promoter proximal regions, after p53 expression, whereas only a weak enrichment pattern was observed for p300 (Figure S2A), thus reinforcing the possibility that the autoacetylated form of p300 is actively associated with p53-mediated transcriptional initiation (Figure 3A). We analyzed the differential occupancy of p300 and ac-p300 with publicly available datasets of RNAPII, H3K27ac (active promoter

mark), and H3K4me1 (enhancer mark) distribution. The abundance of ac-p300 at the promoters correlated with the presence of RNA Pol II enrichment and active promoter marks such as H3K27ac (Figure 3A). These data indicated a specific role for ac-p300 within the entire pool cellular p300. The co-activator occupancy has been integrated with the microarray expression analysis of the p53-induced differentially expressed genes (Jiang et al., 2015), revealing a greater overlap between p53-driven transcription and ac-p300 (4,341 genes) recruitment (Figures 3C and 3D) in comparison with p300 (1950 genes) (Figure 3B).

The Gain-of-Function Mutant p53 Induces p300 Autoacetylation to Enhance Tumorigenesis

The *TP53* gene is mutated in approximately 50% of malignancies, of which 75% are missense mutations (Freed-Pastor and Prives, 2012; Olivier et al., 2010). The missense mutations mapping to the DNA binding domain not only abrogate the tumor suppressive functions of p53 but also impart unique oncogenic functions to the mutant protein (Freed-Pastor and Prives, 2012). Since our previous results elucidated the mechanisms of p53-mediated induction of intermolecular p300 autoacetylation and the role of autoacetylated p300 in p53 downstream gene expression, we investigated whether these GOF mutants retained the ability to enhance p300 catalytic activity through the induction of autoacetylation. We tested different GOF hotspot mutants, three conformational mutants (R175H, V143A, and R249S), and two DNA contact mutants (R273H and R248W), in an *in vitro* autoacetylation assay. All the GOF mutants appeared to enhance p300 autoacetylation *in vitro*, which was comparable with the enhancement observed in the presence of wild-type p53 (Figure 4A). In H1299 cells ectopically expressing GOF p53 mutants, the levels of autoacetylated p300 were checked by immunofluorescence in the mutant p53 transfected cell versus the untransfected cells. The intensity of autoacetylated p300 immunofluorescence staining revealed that the cells expressing the GOF mutants, both DNA contact mutants (Figures S3A and S3B) and conformational mutants (Figures S3C and S3D), appeared to have significantly higher levels of autoacetylated p300 in comparison with the untransfected controls (Figure S3). To understand the pathophysiological relevance of GOF mutant p53-mediated enhancement of p300 autoacetylation, the R273H p53 mutant, which has one of the highest incidences in cancers (6.7%), was chosen for further investigation. To establish that R273H p53 mutant could alter the levels of p300 autoacetylation alone without affecting the overall p300 protein levels, immunofluorescence was performed in H1299 cells ectopically expressing R273H p53. As observed in the earlier immunofluorescence staining, the autoacetylation of p300 increased dramatically in the presence of R273H (Figure 4B, upper panel) while exhibiting a negligible change in the overall p300 protein levels (Figure 4B, lower panel). These data reinforce the fact that similar to wild-type p53, the GOF R273H mutant too, modulates p300 only at the autoacetylation level and does not appear to affect p300 protein stability or expression. As established earlier that increased KAT activity is a direct consequence of p300 autoacetylation, the levels of different p300-specific histone marks were checked, after ectopically expressing the mutant R273H and wild-type p53 as a control. It is evident from the western blotting analysis that histone acetylation on H2AK5 and H3K9 were up-regulated in cells transfected with the mutant and wild-type p53 in comparison with the vector-transfected cells (Figure 4C). To investigate the role of R273H mutant-mediated induction of p300 autoacetylation in regulating the tumorigenic potential of the mutant, an inducible Tet-ON H1299 cell line for R273H p53 expression was created. Earlier experiments have established that the direct interaction of p53 with p300 is essential for the induction of p300 autoacetylation. Therefore, the aim of the experiment was also to test whether the direct interaction of p300 and p53 mutant R273H played a role in the GOF of this mutant. In a wound healing assay, the cells were treated with doxycycline to induce the expression of R273H p53 and the untreated cells served as the experimental controls. Under both conditions, R273H p53 presence and absence, the cells were treated with either the p53-p300 interfering p53 phosphomimic peptide or the control scrambled peptide. On doxycycline treatment the wound created in the control cells healed faster, suggesting that the R273H p53 mutant indeed exhibited GOF properties, marked by higher proliferation and migration. The cells treated with the scrambled peptide showed similar closure time as the control cells, signifying that the scrambled peptide did not have any apparent pleiotropic effect. Interestingly, the cells treated with the phosphomimic p300-p53 interfering peptide migrated and proliferated slower than the control cells, implicating a possible role of p300 interaction in the tumorigenic potential of R273H p53 (Figure 4D). Moreover, the delay in wound closure observed on p53 phosphomimic peptide treatment was comparable with that of the untreated (doxycycline negative) cells, suggesting that the peptide treatment may have abrogated the effect of the p53 mutant expression. Furthermore, in the doxycycline-negative cells, the control, p53 phosphomimic peptide, and scrambled peptide-treated cells migrated and proliferated at similar rates, suggesting that the effect observed on p53 phosphomimic peptide treatment in the doxycycline-treated cells had a direct correlation with the presence of mutant p53 (Figure 4D). Collectively, these results implicate the direct role of

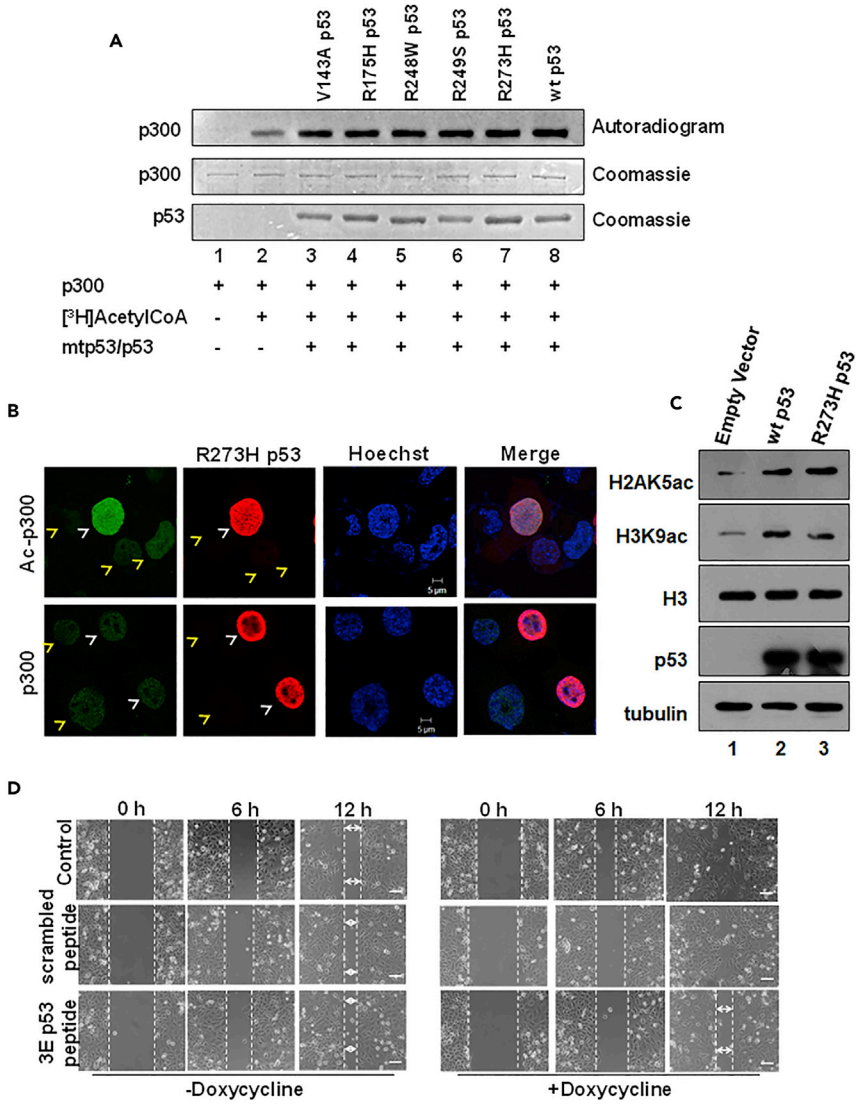

Figure 4. p53 Gain-of-Function (GOF) Mutants Are Inducers of p300 Autoacetylation

(A) An *in vitro* HAT assay was performed to determine the levels of autoacetylation of p300 in the presence of recombinant GOF p53 mutants and wild-type p53.

(B) p53 null H1299 cells were transfected with R273H p53 mutant. The levels of Ac-p300 (autoacetylated p300) (top panel, green), p300 (bottom panel, green), and mutant p53 (red) were determined by immunofluorescence. Transfected cells and untransfected cells are indicated by white and yellow arrows, respectively. Scale bar, 5 μm. (See Figure S3.)

(C) Western blotting analysis was performed to determine the levels of p300-specific histone acetylation levels in H1299 cells transiently transfected with pCMV2 Empty Vector, wild-type p53, and the DNA contact mutant R273H p53. Histone H3 levels served as the loading control.

(D) Representative images (of two biological repeats) of a wound healing assay performed in doxycycline-inducible R273H p53 H1299 stable cell line. The cells were treated with either 10 μM phosphomimic p53 peptide or 10 μM scrambled peptide as indicated with or without doxycycline treatment. Scale bar, 100 μm. (See Figure S4.)

p300 (and possible p300 autoacetylation) in the induction of R273H tumorigenic functions, creating a positive feedback loop between the two proteins. Western blotting analysis was done with the cells used in the assay to ascertain the expression status of R273H p53 in the presence and absence of doxycycline treatment (Figure 4A). Since in the above-mentioned experiment the mutant R273H was artificially expressed in H1299 cells, it was important to demonstrate a similar phenomenon in a cancerous cell line endogenously expressing the R273H p53 mutant. Therefore, a similar wound healing assay was performed in the AW13516 oral cancer cell line, which expresses high levels of the R273H p53 mutant. Similar to the

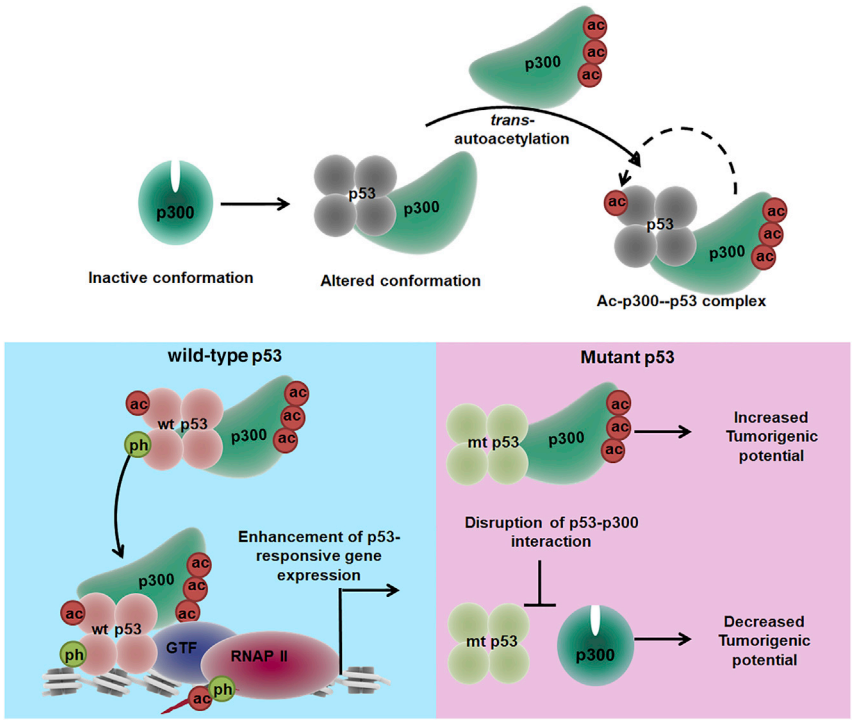

Figure 5. Model Depicting the Physiological Significance of p53-Mediated Enhancement of p300 Autoacetylation

The histone acetyltransferase is present in a "closed" inactive conformation when present in an unbound state, but in the presence of p53, a substantial rearrangement in the domain architecture of p300 is observed. In the p53-bound complex, p300 undergoes a conformational switch from an inactive to an altered conformation. This altered conformational state of p300 is more conducive to intermolecular autoacetylation, a phenomenon that enhances the catalytic activity of p300. When p300 is activated by wild-type p53, there is a re-distribution of autoacetylated p300 onto p53-responsive gene promoters, leading to the downstream tumor suppressive functions of p53, whereas when mutant p53 induces the autoacetylation of p300, we observe an increased tumorigenic potential. The gain-of-function effect of mutant p53 is abrogated when the interaction between mutant p53 and p300 is disrupted.

previous experiment, the p53 phosphomimic peptide drastically impaired the rate of wound closure (Figure S4B, middle panel, 12 h) in comparison with the untreated and scrambled peptide-treated controls (Figure S4B, top and bottom panels, 12 h).

To establish further that the GOF mutant p53-mediated induction of p300 autoacetylation may be an oncogenic pathway through which mutant p53 can exert its tumorigenic potential, we tested whether loss-of-function (LOF) tetramerization-defective mutants could also induce p300 autoacetylation. Tetramerization-defective mutants were transfected into H1299 cells, and the levels of autoacetylated p300 was probed by immunofluorescence. It was found that the p53 tetramerization mutants failed to enhance p300 autoacetylation in the H1299 cells (Figures S5A and S5B). It has been shown earlier that p53 proteins that cannot form tetramers lose their ability to interact with p300 (Itahana et al., 2009). It is fair to assume that the physical interaction of p53 and p300 is a key requisite for the induction of p300 autoacetylation. The L344A p53 tetramerization-defective mutant was tested in an autoacetylation assay. The autoacetylation of p300 does not alter in the presence of the mutant (Figure S5C). When H1299 cells were transfected with the L344A p53 mutant, we observed no enhancement in the global levels of p300 autoacetylation or any alteration in p300 protein levels (Figures S5D and S5E). These experiments revealed the importance of p53 tetramerization and the requirement for the direct interaction between p53 and p300 for p300 autoacetylation and augmentation of its acetyltransferase activity (Figure 5).

DISCUSSION

The functional cross talk between p300 and p53 is well established; however, the role of p53 in the modulation of the enzymatic activity of p300 has not been addressed before. The chromatin

immunoprecipitation sequencing (ChIP-seq) analysis of ac-p300 genome occupancy after p53 induction provided further insights into the transcriptional cascades triggered by effector (p53)-mediated induction of p300 autoacetylation. p300 autoacetylation can control its catalytic activity (Thompson et al., 2004), but the dynamics of p300 autoacetylation under physiological stimuli are not fully understood. The present findings provide experimental evidence that establishes p53 as a *bona fide* modulator of p300 autoacetylation. Remarkably, among all of the substrates of p300 tested, only p53 enhanced p300 autoacetylation, thus confirming the molecular specificity of this phenomenon. The preferential induction of p300 autoacetylation by p53 over that of other acetyltransferases further exhibited the specificity of p53-mediated induction of p300 autoacetylation. This result further suggested that the induction of autoacetylation is not merely a consequence of enzyme-substrate interaction. The structural plasticity of p300 not only increases its interactome but also provides an additional level of regulation for this essential epigenetic enzyme. Thompson et al have shown that the basal catalytic activity of p300 is stimulated through the autoacetylation of certain lysine residues present on the auto-inhibitory loop residing in the KAT domain. It was speculated that, on acetylation of these lysine residues, the loop would be dislodged thereby allowing enhanced catalytic activity (Thompson et al., 2004). Surface-enhanced Raman spectroscopy (SERS)-based structural studies on the minimal p300 HAT domain provided evidence to demonstrate that p300 when hyper-autoacetylated in the presence of acetyl-CoA exhibited a structural reorganization in the HAT domain (Arif et al., 2007). This finding was corroborated by another SERS-based structural study using small molecule activators of p300, CTB and CTPB, which showed a similar structural alteration in the HAT domain (Mantelingu et al., 2007). The 2.8 Å crystal structure of p300 catalytic core domain (bromodomain-RING-PHD-HAT (PDB: 4BHW)) revealed that the bromodomain-RING-PHD domains associate closely with the HAT domain, through several conserved contacts. In the crystal structure, the spatial arrangement of the domains suggests that p300 alone is present in a closed inactive conformation, which the authors speculated could be relieved by inter-molecular autoacetylation (Delvecchio et al., 2013). Studies have indicated that a conformational alteration may be a prerequisite for complete activation of p300 acetyltransferase activity (Delvecchio et al., 2013; Kaypee et al., 2018; Yi et al., 2017). In our recent study, we have shown that the decameric histone chaperone NPM1 could alter the structural conformation of p300, functioning as a molecular chaperone for the intrinsically disordered enzyme thereby inducing p300 autoacetylation and acetyltransferase activity, whereas the disruption of NPM1 oligomerization abrogates its ability to activate p300 (Kaypee et al., 2018). Drawing parallels to this study, we find that p53, in its tetrameric form, is a potent inducer of p300 autoacetylation. On disruption of its tetramers (in tetramerization-defective mutants), p53 appears to lose its ability to enhance p300 autoacetylation. Corroborating the model proposed by Teufel et al., we can conjecture that a single molecule of p300 can wrap around tetrameric p53 (Teufel et al., 2007), as a result of which p300 attains a conformation that may be conducive to intermolecular autoacetylation, as opposed to the closed inactive conformation observed in the crystal structure of the catalytic core of p300 (Delvecchio et al., 2013). However, the conformational alterations should be further validated through extensive structural studies on the full-length p300-p53 complex. This model may have further implications on the recruitment of p300/CBP to chromatin.

p300/CBP is recruited to gene promoters by several transcription factors (An et al., 2004; Kundu et al., 2000) where it can assemble transcription complexes that facilitate gene expression. The autoacetylation of p300 has been proposed to induce distinct structural changes that are critical for its activity. Black *et al*. have shown that the presence of p300 at the preinitiation complex (PIC) exerts an inhibitory effect of transcription *in vitro*. The release of p300 from the complex is attributed to the possible conformational switch in the p300 structure after autoacetylation (Black et al., 2006). It is clear from this study that p300 autoacetylation is essential for maximal transcription to proceed. The predominant occupancy of ac-p300 on the TSS of the promoters is a novel finding based on the obtained ChIP-seq analysis. These data are in agreement with the factor-dependent recruitment of the acetyltransferases p300/CBP and subsequent gene activation, as previously reported. Evident from our biochemical data, the direct interaction of p53 with its co-activator p300/CBP is functionally important in this process and serves as the mechanism of induction of autoacetylation. Ceschin et al. have shown that CBP is methylated at multiple sites by the arginine methyltransferase protein CARM1 and the arginine methylation of CBP stimulates CBP activity through the induction of CBP autoacetylation. Use of polyclonal antibodies recognizing specific CBP methylation species has indicated that each methylated class of CBP has differential HAT activities and distinct transcriptional effects, thereby diversifying the estrogen receptor response (Ceschin et al., 2011). The contextual recruitment of p300 has been noted in another study performed in the MCF7 cell line, in which it has been observed that, in resting cells, p300 appears to show a preference toward neural lineage gene promoters, whereas the

enrichment of p300 shifts toward estrogen-regulated gene targets after estradiol treatment (Wang and Li, 2016). In a recent report, CBP has been shown to interact with RNAs. At active enhancers, CBP interacts with enhancer RNAs, which bind to the CBP catalytic domain, inducing CBP autoacetylation (Bose et al., 2017). The resultant enhancement in CBP activity leads to increased histone acetylation and expression of target genes. In the present work, the differential occupancy of p300 and ac-p300 was investigated after p53 activation. After autoacetylation, in the presence of p53, p300 appeared to show a strong preference for the TSS (Figure 3A and S2A), in agreement with the recruitment model discussed earlier. The binding of ac-p300 was strongly associated with RNA Pol II occupancy and the promoter acetylation mark H3K27ac. This finding suggested that ac-p300 is indeed involved in the assembly of the basal transcription machinery at promoter-proximal regions of genes. The overall pool of p300 did not show an appreciable alteration in chromatin occupancy in the presence of p53, whereas a distinct redistribution in ac-p300 enrichment was observed. Notably, the integration of the ChIP-seq data with the gene expression microarray analysis revealed that the enrichment of ac-p300 was a better determinant of p53-mediated gene expression than the presence of unmodified p300. This result was in agreement with previous studies in which p300 has been shown to occupy transcriptionally silent regions or the chromatin, whereas the co-occupancy of (presumably autoacetylated) p300 with its histone acetylation mark H3K27ac was observed at transcriptionally active genes (Holmqvist and Mannervik, 2013). With the current evidence, it can be speculated that the ability to induce structural alterations in p300, leading to enhancement of its acetyltransferase activity, may be a key determinant in p300 chromatin recruitment and downstream transcriptional programs. The ChIP-seq data suggest that the phenomenon of factor-induced p300 autoacetylation may play a pivotal role in the integration of stimulus-driven transcriptional pathways. Specifically, the recruitment of the catalytically active form of p300 may trigger a rapid transcriptional response to internal and external signaling cues. In this study, it is the p53-driven pathway that stimulates a burst in ac-p300 levels and an alteration of the epigenetic landscape, which may be essential for these p53 signaling pathways. We hypothesize that after p53 is stabilized in the cell or overexpressed, it associates with its ubiquitously expressed co-activator p300. This association triggers a conformational alteration in p300, thereby potentiating intermolecular autoacetylation. It is this catalytically active form of p300 that is subsequently enriched in p53-target gene regulatory chromatin regions via its interaction with p53. The active ac-p300 then acetylates histone tails at these loci, decompacting chromatin and leading to enhanced transcription p53-dependent and (possibly) independent gene networks (Figure 5, Table S2).

A large proportion of tumors harbor mutations in p53 that nullify specific DNA-binding properties. A subset of these mutants, the GOF mutants, also gain aggressive proliferation properties, and it is now known that this is achieved by relocation to regulatory regions of genes responsible for proliferation and drug resistance followed by activation of expression of those genes. The results presented here underline that, in spite of the loss of DNA-binding properties, these mutants retain their ability to activate the co-activator p300 through the induction of autoacetylation, thus promoting the activation of these growth-promoting genes in the new locale. Abolition of the GOF properties by a site-directed peptide inhibitor of p53-p300 interaction suggests that these classes of inhibitors may offer promise against tumors bearing aggressive GOF mutant p53 alleles (Figure 5).

The activation of p300 by p53 suggests that p300 may be preferentially activated when it is recruited to p53 at its target sites. This activation would suggest an enhanced activity of p300 when it is complexed with target-site-bound p53, thereby leading to localized transcriptional initiation. Thus, the augmented activity of p300 at genes to which it is recruited by p53 adds another element of specificity beyond that of the transcription factor binding. Moreover, p53 was able to modulate the levels of histone acetylation concomitant with the induction of p300 autoacetylation, thus signifying that the tumor suppressor p53 can alter the epigenetic landscape through the regulation of p300 acetyltransferase activity. We speculate that the activation of p300 by p53 demonstrated here may be a representative example of a general mechanism for attaining the high degree of spatiotemporal specificity required for attaining exquisite and intricate gene regulation.

METHODS

All methods can be found in the accompanying Transparent Methods supplemental file.

DATA AND SOFTWARE AVAILABILITY

p300 and ac-p300 ChIP-seq data, SRA: SRR5831017.

SUPPLEMENTAL INFORMATION

Supplemental Information includes Transparent Methods, five figures, and three tables and can be found with this article online at https://doi.org/10.1016/j.isci.2018.06.002.

ACKNOWLEDGMENTS

This work was supported by Jawaharlal Nehru Center for Advanced Scientific Research (JNCASR) (MBGU/TKK), Sir JC Bose Fellowship, Department of Science and Technology, Government of India (SR/S2/JCB-28/2010) and Virtual National Oral Cancer Institute, Department of Biotechnology, Government of India (BT/PR17576/MED/30/1690/2016). T.K.K. is a Sir JC Bose Fellow. We acknowledge Mr. Madavan Vasudevan and Ms. Madhura Tathode, Bionivid Technology Pvt. Ltd., for the ChIP-seq analysis. We acknowledge Dr. Dirk Gründemann (University of Cologne, Germany) for the pEBTetD SLC22A1 construct. We acknowledge Dr. Amit Dutt (ACTREC, Mumbai, India) for the AW13516 cell line. We acknowledge the Confocal Imaging Facility at JNCASR. We have used illustration templates from the website somersault1824 (http://www.somersault1824.com) available under a Creative Commons Attribution-Noncommercial-Share Alike license (CC BY-NC-SA 4.0) in the Model (Figure 5) and Graphical Abstract.

AUTHOR CONTRIBUTIONS

T.K.K. and S.K. have conceived the project. T.K.K., S.K., and S.R. have written the manuscript. S.K., S.A.S., and S.P. have executed the molecular biology experiments. P.G. and N.S.R. have synthesized and characterized the peptides used in this study.

DECLARATION OF INTERESTS

The authors declare no competing interests.

Received: December 21, 2017
Revised: January 18, 2018
Accepted: June 4, 2018
Published: June 29, 2018

REFERENCES

An, W., Kim, J., and Roeder, R.G. (2004). Ordered cooperative functions of PRMT1, p300, and CARM1 in transcriptional activation by p53. Cell *117*, 735–748.

Arif, M., Kumar, G.V.P., Narayana, C., and Kundu, T.K. (2007). Autoacetylation induced specific structural changes in histone acetyltransferase domain of p300: probed by surface enhanced Raman spectroscopy. J. Phys. Chem. B *111*, 11877–11879.

Arif, M., Vedamurthy, B.M., Choudhari, R., Ostwal, Y.B., Mantelingu, K., Kodaganur, G.S., and Kundu, T.K. (2010). Nitric oxide-mediated histone hyperacetylation in oral cancer: target for a water-soluble HAT inhibitor, CTK7A. Chem. Biol. *17*, 903–913.

Barlev, N.A., Liu, L., Chehab, N.H., Mansfield, K., Harris, K.G., Halazonetis, T.D., and Berger, S.L. (2001). Acetylation of p53 activates transcription through recruitment of coactivators/histone acetyltransferases. Mol. Cell *8*, 1243–1254.

Bedford, D.C., Kasper, L.H., Fukuyama, T., and Brindle, P.K. (2010). Target gene context influences the transcriptional requirement for the KAT3 family of CBP and p300 histone acetyltransferases. Epigenetics *5*, 9–15.

Bieging, K.T., Mello, S.S., and Attardi, L.D. (2014). Unravelling mechanisms of p53-mediated tumour suppression. Nat. Rev. Cancer *14*, 359–370.

Black, J.C., Choi, J.E., Lombardo, S.R., and Carey, M. (2006). A mechanism for coordinating chromatin modification and preinitiation complex assembly. Mol. Cell *23*, 809–818.

Black, J.C., Mosley, A., Kitada, T., Washburn, M., and Carey, M. (2008). The SIRT2 deacetylase regulates autoacetylation of p300. Mol. Cell *32*, 449–455.

Bose, D.A., Donahue, G., Reinberg, D., Shiekhattar, R., Bonasio, R., and Berger, S.L. (2017). RNA binding to CBP stimulates histone acetylation and transcription. Cell *168*, 135–149.e22.

Ceschin, D.G., Walia, M., Wenk, S.S., Duboé, C., Gaudon, C., Xiao, Y., Fauquier, L., Sankar, M., Vandel, L., and Gronemeyer, H. (2011). Methylation specifies distinct estrogen-induced binding site repertoires of CBP to chromatin. Genes Dev. *25*, 1132–1146.

Chan, H.M., and La Thangue, N.B. (2001). p300/CBP proteins: HATs for transcriptional bridges and scaffolds. J. Cell Sci. *114*, 2363–2373.

Delvecchio, M., Gaucher, J., Aguilar-Gurrieri, C., Ortega, E., and Panne, D. (2013). Structure of the p300 catalytic core and implications for chromatin targeting and HAT regulation. Nat. Struct. Mol. Biol. *20*, 1040–1046.

Dulac, C. (2010). Brain function and chromatin plasticity. Nature *465*, 728–735.

Dyson, H.J., and Wright, P.E. (2016). Role of intrinsic protein disorder in the function and interactions of the transcriptional coactivators CREB-binding protein (CBP) and p300. J. Biol. Chem. *291*, 6714–6722.

Espinosa, J.M., and Emerson, B.M. (2001). Transcriptional regulation by p53 through intrinsic DNA/chromatin binding and site-directed cofactor recruitment. Mol. Cell *8*, 57–69.

Freed-Pastor, W.A., and Prives, C. (2012). Mutant p53: one name, many proteins. Genes Dev. *26*, 1268–1286.

Gu, W., and Roeder, R.G. (1997). Activation of p53 sequence-specific DNA binding by acetylation of the p53 C-terminal domain. Cell *90*, 595–606.

Haaland, I., Opsahl, J.A., Berven, F.S., Reikvam, H., Fredly, H.K., Haugse, R., Thiede, B., McCormack, E., Lain, S., Bruserud, Ø., et al. (2014). Molecular mechanisms of nutlin-3 involve acetylation of p53, histones and heat shock proteins in acute myeloid leukemia. Mol. Cancer *13*, 116.

Hansson, M.L., Popko-Ścibor, A.E., Saint Just Ribeiro, M., Dancy, B.M., Lindberg, M.J., Cole, P.A., and Wallberg, A.E. (2009). The transcriptional coactivator MAML1 regulates p300 autoacetylation and HAT activity. Nucleic Acids Res. *37*, 2996–3006.

Holmqvist, P.-H., and Mannervik, M. (2013). Genomic occupancy of the transcriptional co-activators p300 and CBP. Transcription *4*, 18–23.

Itahana, Y., Ke, H., and Zhang, Y. (2009). p53 Oligomerization is essential for its C-terminal lysine acetylation. J. Biol. Chem. *284*, 5158–5164.

Jiang, L., Kon, N., Li, T., Wang, S.-J., Su, T., Hibshoosh, H., Baer, R., and Gu, W. (2015). Ferroptosis as a p53-mediated activity during tumour suppression. Nature *520*, 57–62.

Kaypee, S., Sahadevan, S.A., Sudarshan, D., Halder Sinha, S., Patil, S., Senapati, P., Kodaganur, G.S., Mohiyuddin, A., Dasgupta, D., and Kundu, T.K. (2018). Oligomers of human histone chaperone NPM1 alter p300/KAT3B folding to induce autoacetylation. Biochim. Biophys. Acta *1862*, 1729–1741.

Kim, W.J., Rivera, M.N., Coffman, E.J., and Haber, D.A. (2012). The WTX tumor suppressor enhances p53 acetylation by CBP/p300. Mol. Cell *45*, 587–597.

Kitagawa, M., Lee, S.H., and McCormick, F. (2008). Skp2 Suppresses p53-dependent apoptosis by inhibiting p300. Mol. Cell *29*, 217–231.

Krois, A.S., Ferreon, J.C., Martinez-Yamout, M.A., Dyson, H.J., and Wright, P.E. (2016). Recognition of the disordered p53 transactivation domain by the transcriptional adapter zinc finger domains of CREB-binding protein. Proc. Natl. Acad. Sci. USA *113*, E1853–E1862.

Kumazawa, T., Nishimura, K., Kuroda, T., Ono, W., Yamaguchi, C., Katagiri, N., Tsuchiya, M., Masumoto, H., Nakajima, Y., Murayama, A., et al. (2011). Novel nucleolar pathway connecting intracellular energy status with p53 activation. J. Biol. Chem. *286*, 20861–20869.

Kundu, T.K., Palhan, V.B., Wang, Z., An, W., Cole, P.A., and Roeder, R.G. (2000). Activator-dependent transcription from chromatin in vitro involving targeted histone acetylation by p300. Mol. Cell *6*, 551–561.

Lambert, P.F., Kashanchi, F., Radonovich, M.F., Shiekhattar, R., and Brady, J.N. (1998). Phosphorylation of p53 serine 15 increases interaction with CBP. J. Biol. Chem. *273*, 33048–33053.

Lee, C.W., Sørensen, T.S., Shikama, N., and La Thangue, N.B. (1998). Functional interplay between p53 and E2F through co-activator p300. Oncogene *16*, 2695–2710.

Lee, C.W., Arai, M., Martinez-Yamout, M.A., Dyson, H.J., and Wright, P.E. (2009). Mapping the interactions of the p53 transactivation domain with the KIX domain of CBP. Biochemistry *48*, 2115–2124.

Lee, C.W., Ferreon, J.C., Ferreon, A.C.M., Arai, M., and Wright, P.E. (2010). Graded enhancement of p53 binding to CREB-binding protein (CBP) by multisite phosphorylation. Proc. Natl. Acad. Sci. USA *107*, 19290–19295.

Levine, M., and Tjian, R. (2003). Transcription regulation and animal diversity. Nature *424*, 147–151.

Lill, N.L., Grossman, S.R., Ginsberg, D., DeCaprio, J., and Livingston, D.M. (1997). Binding and modulation of p53 by p300/CBP coactivators. Nature *387*, 823–827.

Liu, L., Scolnick, D.M., Trievel, R.C., Zhang, H.B., Marmorstein, R., Halazonetis, T.D., and Berger, S.L. (1999). p53 sites acetylated in vitro by PCAF and p300 are acetylated in vivo in response to DNA damage. Mol. Cell. Biol. *19*, 1202–1209.

Mantelingu, K., Kishore, A.H., Balasubramanyam, K., Kumar, G.V.P., Altaf, M., Swamy, S.N., Selvi, R., Das, C., Narayana, C., Rangappa, K.S., et al. (2007). Activation of p300 histone acetyltransferase by small molecules altering enzyme structure: probed by surface-enhanced Raman spectroscopy. J. Phys. Chem. B *111*, 4527–4534.

Ogryzko, V.V., Schiltz, R.L., Russanova, V., Howard, B.H., and Nakatani, Y. (1996). The transcriptional coactivators p300 and CBP are histone acetyltransferases. Cell *87*, 953–959.

Olivier, M., Hollstein, M., and Hainaut, P. (2010). TP53 mutations in human cancers: origins, consequences, and clinical use. Cold Spring Harb. Perspect. Biol. *2*, a001008.

Perissi, V., Dasen, J.S., Kurokawa, R., Wang, Z., Korzus, E., Rose, D.W., Glass, C.K., and Rosenfeld, M.G. (1999). Factor-specific modulation of CREB-binding protein acetyltransferase activity. Proc. Natl. Acad. Sci. USA *96*, 3652–3657.

Polley, S., Guha, S., Roy, N.S., Kar, S., Sakaguchi, K., Chuman, Y., Swaminathan, V., Kundu, T., and Roy, S. (2008). Differential recognition of phosphorylated transactivation domains of p53 by different p300 domains. J. Mol. Biol. *376*, 8–12.

Reed, S.M., and Quelle, D.E. (2014). p53 acetylation: regulation and consequences. Cancers (Basel) *7*, 30–69.

Rokudai, S., Laptenko, O., Arnal, S.M., Taya, Y., Kitabayashi, I., and Prives, C. (2013). MOZ increases p53 acetylation and premature senescence through its complex formation with PML. Proc. Natl. Acad. Sci. USA *110*, 3895–3900.

Sakaguchi, K., Herrera, J.E., Saito, S., Miki, T., Bustin, M., Vassilev, A., Anderson, C.W., and Appella, E. (1998). DNA damage activates p53 through a phosphorylation-acetylation cascade. Genes Dev. *12*, 2831–2841.

Schneider, R., and Grosschedl, R. (2007). Dynamics and interplay of nuclear architecture, genome organization, and gene expression. Genes Dev. *21*, 3027–3043.

Sen, N., Hara, M.R., Kornberg, M.D., Cascio, M.B., Bae, B.-I., Shahani, N., Thomas, B., Dawson, T.M., Dawson, V.L., Snyder, S.H., et al. (2008). Nitric oxide-induced nuclear GAPDH activates p300/CBP and mediates apoptosis. Nat. Cell Biol. *10*, 866–873.

Shi, D., Dai, C., Qin, J., and Gu, W. (2016). Negative regulation of the p300-p53 interplay by DDX24. Oncogene *35*, 528–536.

Sykes, S.M., Mellert, H.S., Holbert, M.A., Li, K., Marmorstein, R., Lane, W.S., and McMahon, S.B. (2006). Acetylation of the p53 DNA-binding domain regulates apoptosis induction. Mol. Cell *24*, 841–851.

Tang, Y., Luo, J., Zhang, W., and Gu, W. (2006). Tip60-dependent acetylation of p53 modulates the decision between cell-cycle arrest and apoptosis. Mol. Cell *24*, 827–839.

Teufel, D.P., Freund, S.M., Bycroft, M., and Fersht, A.R. (2007). Four domains of p300 each bind tightly to a sequence spanning both transactivation subdomains of p53. Proc. Natl. Acad. Sci. USA *104*, 7009–7014.

Thompson, P.R., Wang, D., Wang, L., Fulco, M., Pediconi, N., Zhang, D., An, W., Ge, Q., Roeder, R.G., Wong, J., et al. (2004). Regulation of the p300 HAT domain via a novel activation loop. Nat. Struct. Mol. Biol. *11*, 308–315.

Turnell, A.S., Stewart, G.S., Grand, R.J.A., Rookes, S.M., Martin, A., Yamano, H., Elledge, S.J., and Gallimore, P.H. (2005). The APC/C and CBP/p300 cooperate to regulate transcription and cell-cycle progression. Nature *438*, 690–695.

Vasudevarao, M.D., Mizar, P., Kumari, S., Mandal, S., Siddhanta, S., Swamy, M.M.M., Kaypee, S., Kodihalli, R.C., Banerjee, A., Naryana, C., et al. (2014). Naphthoquinone-mediated inhibition of lysine acetyltransferase KAT3B/p300, basis for non-toxic inhibitor synthesis. J. Biol. Chem. *289*, 7702–7717.

Vo, N., and Goodman, R.H. (2001). CREB-binding protein and p300 in transcriptional regulation. J. Biol. Chem. *276*, 13505–13508.

Wang, X., and Li, S. (2016). [Corrigendum] Chromatin immunoprecipitation-sequencing predicts p300 binding sites in the MCF7 human breast cancer cell line. Int. J. Mol. Med. *38*, 675.

Yi, P., Wang, Z., Feng, Q., Chou, C.-K., Pintilie, G.D., Shen, H., Foulds, C.E., Fan, G., Serysheva, I., Ludtke, S.J., et al. (2017). Structural and functional impacts of ER coactivator sequential recruitment. Mol. Cell *67*, 733–743.e4.

ISCI, Volume *4*

Supplemental Information

Mutant and Wild-Type Tumor Suppressor p53 Induces p300 Autoacetylation

Stephanie Kaypee, Smitha Asoka Sahadevan, Shilpa Patil, Piya Ghosh, Neeladri Sekhar Roy, Siddhartha Roy, and Tapas K. Kundu

Figure S1

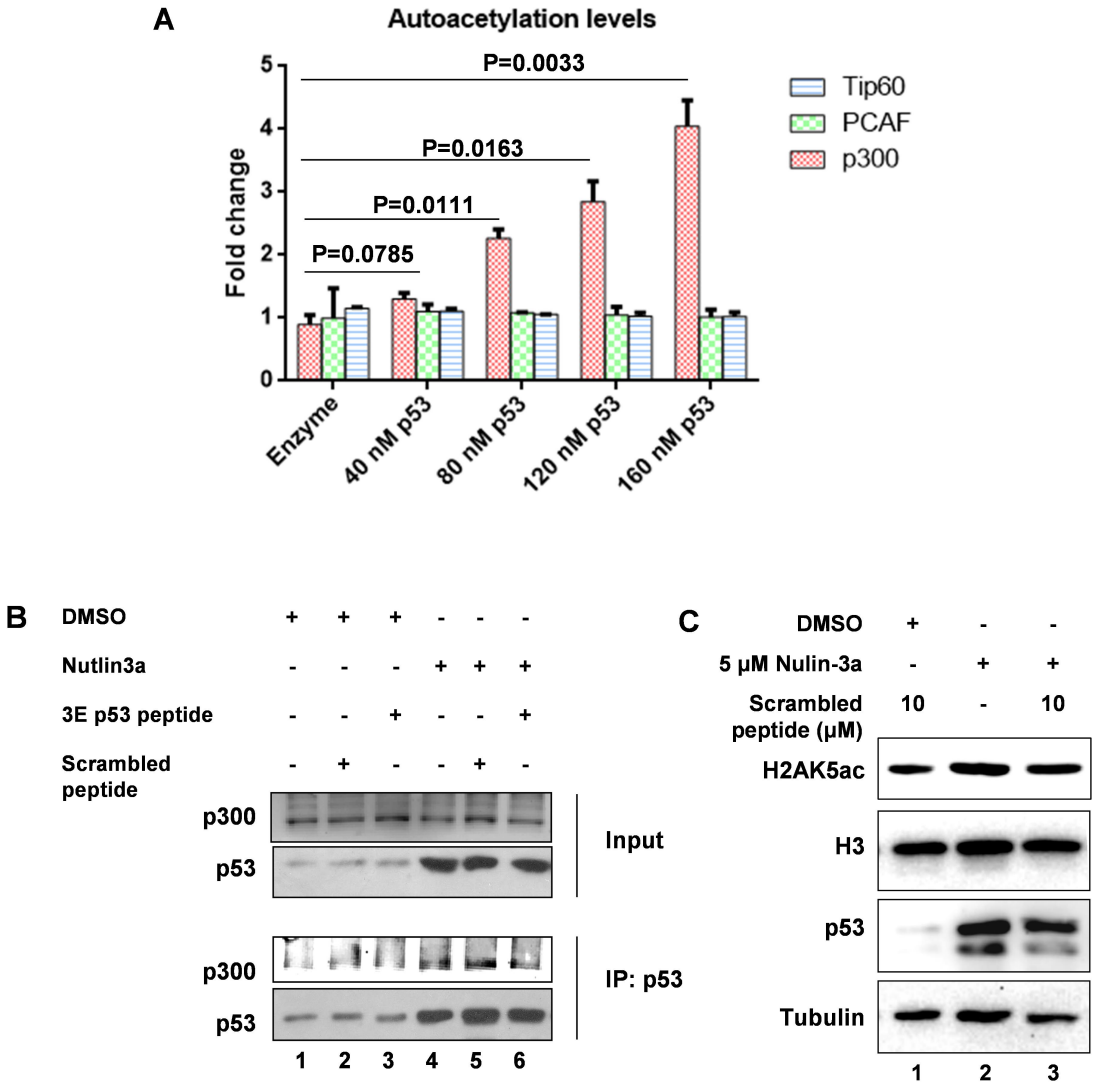
A
Autoacetylation levels
P=0.0033
P=0.0163
P=0.0111
P=0.0785
Fold change
Tip60
PCAF
p300
Enzyme
40 nM p53
80 nM p53
120 nM p53
160 nM p53
B
DMSO
Nutlin3a
3E p53 peptide
Scrambled peptide
p300
p53
Input
IP: p53
1 2 3 4 5 6
C
DMSO
5 μM Nulin-3a
Scrambled peptide (μM)
H2AK5ac
H3
p53
Tubulin
1 2 3

Figure S2

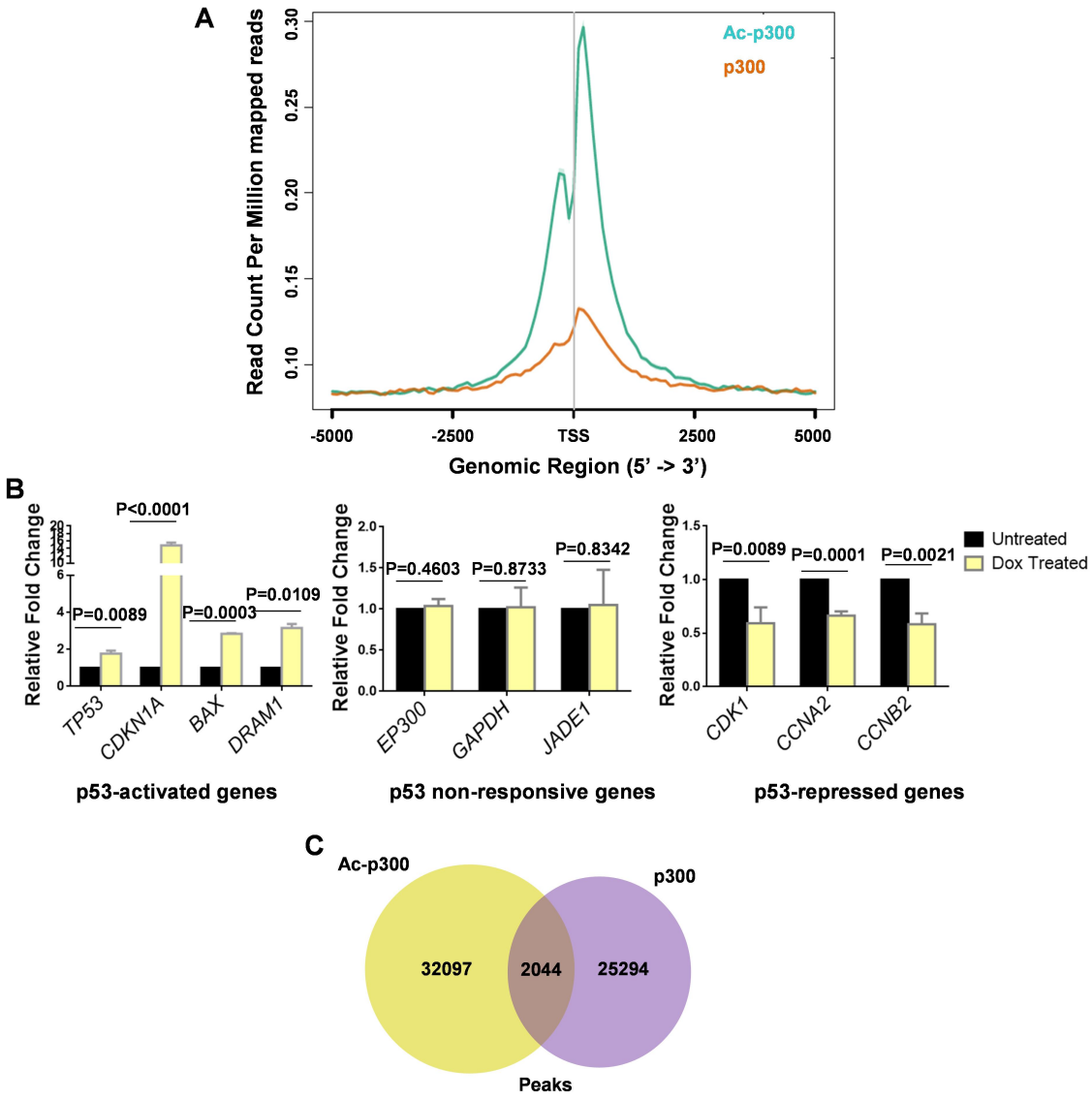
A
Ac-p300
p300
Read Count Per Million mapped reads
0.10
0.15
0.20
0.25
0.30
-5000
-2500
TSS
2500
5000
Genomic Region (5' -> 3')
B
Relative Fold Change
P<0.0001
P=0.0089
P=0.0003
P=0.0109
TP53
CDKN1A
BAX
DRAM1
p53-activated genes
P=0.4603
P=0.8733
P=0.8342
EP300
GAPDH
JADE1
p53 non-responsive genes
P=0.0089
P=0.0001
P=0.0021
CDK1
CCNA2
CCNB2
p53-repressed genes
Untreated
Dox Treated
C
Ac-p300
p300
32097
2044
25294
Peaks

Figure S3

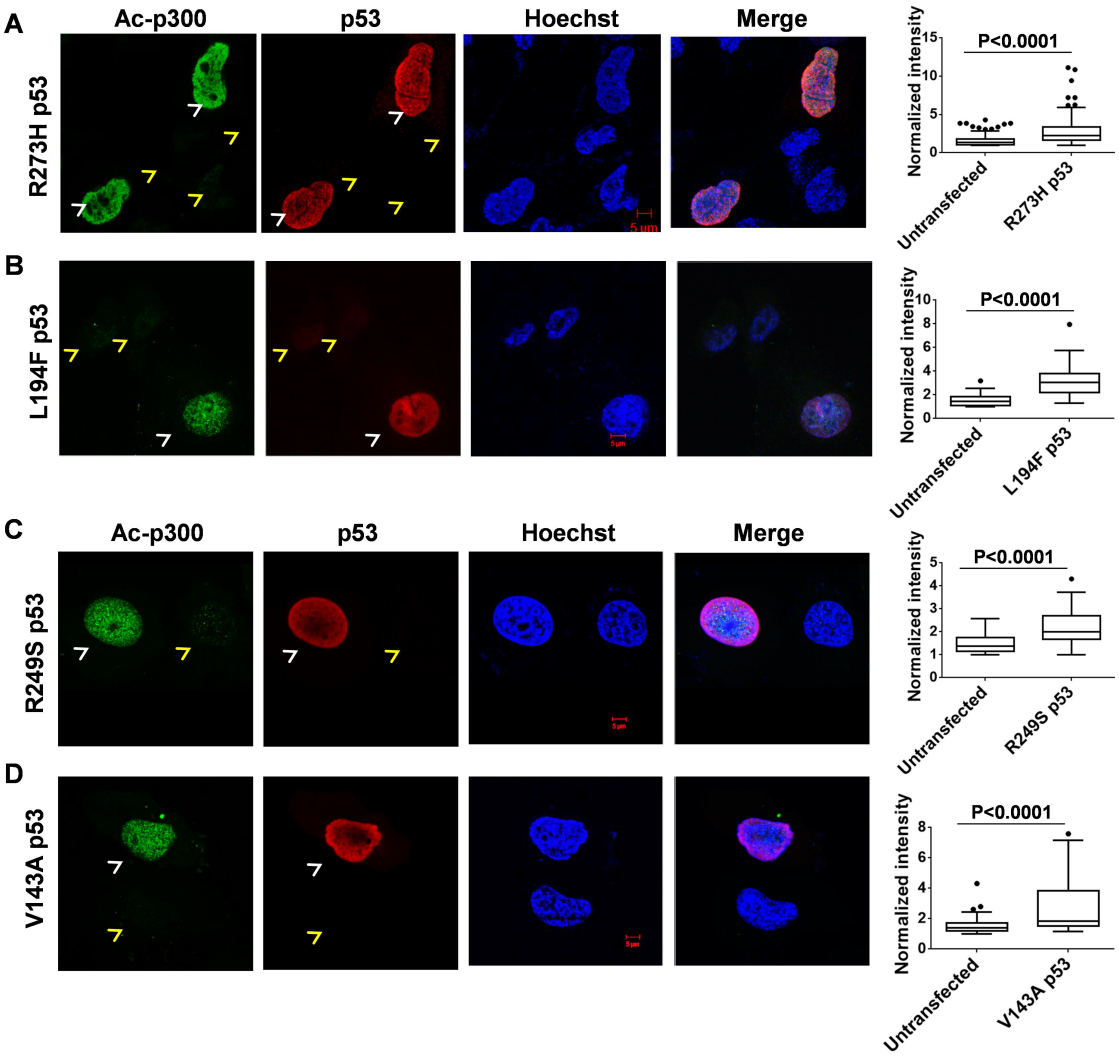
A
Ac-p300
p53
Hoechst
Merge
R273H p53
P<0.0001
Normalized intensity
Untransfected
R273H p53
B
L194F p53
P<0.0001
Normalized intensity
Untransfected
L194F p53
C
Ac-p300
p53
Hoechst
Merge
R249S p53
P<0.0001
Normalized intensity
Untransfected
R249S p53
D
V143A p53
P<0.0001
Normalized intensity
Untransfected
V143A p53

Figure S4

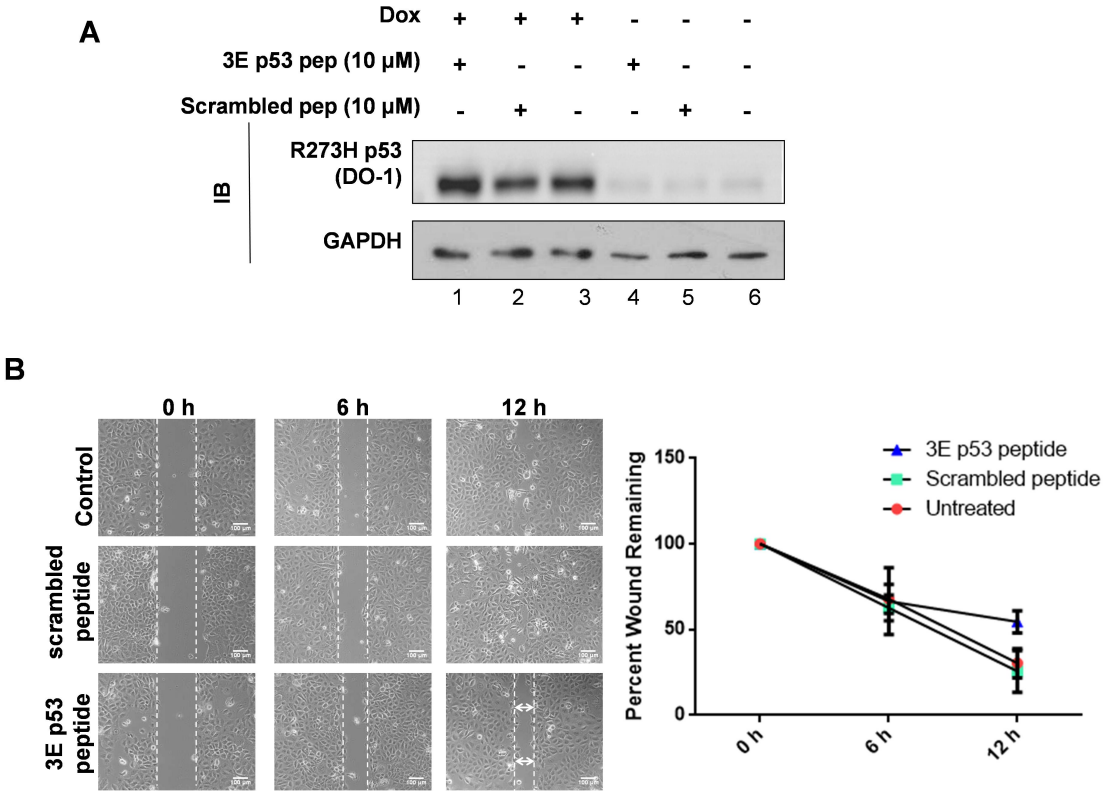
A
Dox + + + - - -
3E p53 pep (10 μM) + - - + - -
Scrambled pep (10 μM) - + - - + -
IB
R273H p53 (DO-1)
GAPDH
1 2 3 4 5 6
B
0 h
6 h
12 h
Control
scrambled peptide
3E p53 peptide
Percent Wound Remaining
150
100
50
0
3E p53 peptide
Scrambled peptide
Untreated
0 h
6 h
12 h

Figure S5

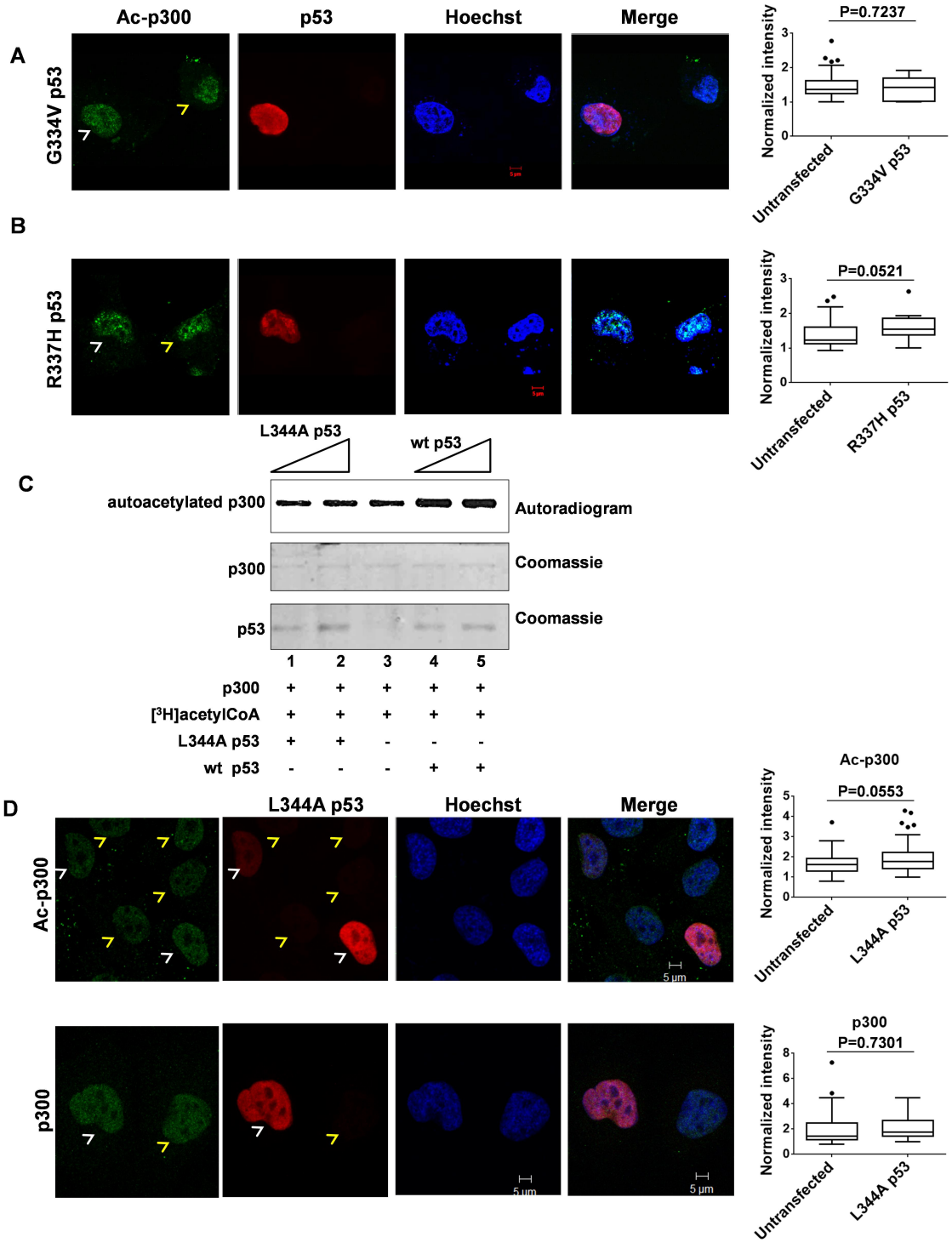
A
Ac-p300
p53
Hoechst
Merge
G334V p53
P=0.7237
Normalized intensity
Untransfected
G334V p53
B
R337H p53
P=0.0521
Normalized intensity
Untransfected
R337H p53
C
L344A p53
wt p53
autoacetylated p300
Autoradiogram
p300
Coomassie
p53
Coomassie
1 2 3 4 5
p300 + + + + +
[3H]acetylCoA + + + + +
L344A p53 + + - - -
wt p53 - - - + +
D
L344A p53
Hoechst
Merge
Ac-p300
Ac-p300
P=0.0553
Normalized intensity
Untransfected
L344A p53
p300
p300
P=0.7301
Normalized intensity
Untransfected
L344A p53
5 µm

Supplemental Figure Legends

Figure S1: Tumor suppressor p53 is an inducer of p300 autoacetylation and function. Related to Figures 1 and 2.

(A) Graphical representation of the mean fold change ± SD of the levels of autoacetylation of each KAT, i.e. p300, PCAF, and Tip60 (see Figure 1A), measured by the relative band intensities measured in ImageJ software, statistical analysis was performed using Unpaired Two-tailed Student's t-test, N=3.

(B) Results of an interaction study between p53-p300 in HepG2 cells treated with DMSO or 5 μM Nutlin-3a and 10 μM p53 phosphomimic (3E p53 peptide) or 10 μM scrambled peptides as indicated. p53 was immunoprecipitated and the co-immunoprecipitated p300 was detected by western blotting analysis.

(C) Immunoblots showing the levels of H2AK5ac, H3, and p53 in HepG2 cells treated with 10 μM scrambled control peptide. Tubulin was used as the loading control.

Figure S2:Validation of theTet-ON wild type p53 expression cell line. Related to Figure 3.

(A) Comparison of the average ChIP-seq enrichment of p300 (orange) and Ac-p300 (cyan)

(B) Validation of p53 activated, repressed and non-responsive genes through RT-qPCR in the doxycycline-inducible wild type p53 stable expression cell line. The mean relative fold changes of the transcript levels ± SD have been plotted. Statistical analysis performed is Unpaired Two-tailed Student's t-test, p-values have been indicated in the figures. (N=3)

(C) Venn Diagram showing the overlap between the ChIP-seq peaks of Ac-p300 and p300 (See Table S2).

Figure S3:p53 GOF mutants are inducers of p300 autoacetylation. Related to Figure 4.

(A-D) H1299 cells were transfected with DNA contact p53 mutants (A) R273H, and (B) L194F, and conformational p53 mutants (C) V143A, and (D) R249S. The levels of Ac-p300 levels were determined in untrasfected cells versus mutant p53 transfected cells in p53 null H1299 cell line by immunofluorescence. Fluorescence intensity of Ac-p300 in untransfected versus p53 transfected cells have been quantified and represented as a Tukey Box and Whiskers plot (median ± SD). Statistical analysis performed is Unpaired Two-tailed Student's t test, p-values have been mentioned in

the figure (n=50 cells from three independent experiments). Transfected cells and untransfected cells are indicated by white and yellow arrows respectively. Scale bar, 5 μm.

Figure S4: Disruption of R273H p53- p300 interaction compromises R273H p53 Gain-of-Function in cancer cells. Related to Figure 4.

(A) Immunoblots to determine the expression of mutant p53 in cells under the different condition of the experiment (See Figure 4D).

(B) Representative images of a wound healing assay performed in AW13516 oral cancer cells expressing p53 mutant, R273H. The cells were treated with 20 μM scrambled or p53 phosphomimic peptide. Untreated cells have been designated as Control. The wound width was measured and represented as percent wound remaining, plotted as mean ± SEM. N=2. Scale bar, 100 μm.

Figure S5:Tetramerization-defectivep53 mutants fail to enhance p300 autoacetylation in cells. Related to Figure 4.

(A)& (B) p53 null H1299 cells were transfected with (A) G344A, and (B) R337H as indicated. The levels of K1499ac p300 and mutant p53 were determined in untrasfected versus mutant p53 transfected cells in p53 null H1299 cell line by immunofluorescence. Fluorescence intensity of Ac-p300 in untransfected versus p53 transfected cells have been quantified (and represented as a Tukey Box and Whiskers plot (median ± SD)). Statistical analysis performed is Unpaired Two-tailed Student's t-test, p-values have been indicated in the figures (n=50 cells from three independent experiments). Transfected cells and untransfected cells are indicated by white and yellow arrows respectively. Scale bar, 5 μm.

(C) An in vitro autoacetylation assay was performed to determine the effect of tetramerization L344A p53 mutant on the induction of p300 autoacetylation. 20 nM p300, 80 nM and 120 nM of L344A p53 or wild type p53 was used respectively. The autoradiogram depicts the levels of autoacetylated p300, the CBB staining shows the loading controls.

(D) & (E) In H1299 cells tetramerization mutant L344A p53 was exogenously expressed and the levels of (D) Ac-p300 and (E) p300 were determined by immunofluorescence. Fluorescence intensity of Ac-p300, and p300 was measured in untransfected versus

p53 transfected cells (and represented as a Tukey Box and Whiskers plot (median ± SD)). Statistical analysis performed is Unpaired Two-tailed Student's t-test, p-values have been indicated in the figures (n=50 cells from three independent experiments). Transfected cells and untransfected cells are indicated by white and yellow arrows respectively. Scale bar, 5 μm.

Supplemental Tables

Table S1. Peptide sequences (Related to Figures 2, 4, S1, and S4)

p53 11-30 phosphomimic (S15E,T18E, S20E) [3E p53 peptide/ p53 phosphomimic peptide]	PKKKRKVRRRRRREPPLEQEEFE DLWKLLPENN
p53 11-30 phosphomimic scrambled [scrambled peptide]	PKKKRKVRRRRRRLLQLEPEELEPKFEWNPDEN

Table S2. Pathway analysis of up-regulated genes unique to Ac-p300 occupancy. (Related to Figure 3)

Term	No. of genes	p-value
endoplasmic reticulum membrane	**28**	**0.00049052**
Apoptosis	**7**	**0.00090694**
Mitochondrion	**30**	**0.00123927**
endoplasmic reticulum	**26**	**0.00131164**
Transit peptide	**18**	**0.00172177**
extrinsic apoptotic signaling pathway via death domain receptors	**5**	**0.00322367**
Mitochondrion	**34**	**0.00578275**
Ribonucleoprotein	**11**	**0.00971273**
GTP-binding	**12**	**0.01009015**
Serine/threonine-protein kinase	**13**	**0.01049547**
Acyltransferase	**8**	**0.01105162**
tumor necrosis factor-mediated signaling pathway	**7**	**0.01246378**
ER to Golgi vesicle-mediated transport	**8**	**0.01554622**

integrator complex	**3**	**0.01696651**
Transferase	**36**	**0.01702659**
Citrate cycle (TCA cycle)	**4**	**0.01714417**
response to lipopolysaccharide	**8**	**0.01757149**
snRNA processing	**3**	**0.01812607**
activation of cysteine-type endopeptidase activity involved in apoptotic signaling pathway	**3**	**0.01812607**

Table S3. List of primers (Related to Figures 2, 3 and S2)

	Forward Primer (5'-3')	Reverse Primer (5'-3')
Cloning Primers		
pFLAG-CMV™-2 p53	CCCAAGCTTATGGAGGAGCCGCAGTC	CGCGGATCCTCAGTCTGAGTCAGGC
pEBTetD p53/ R273H p53	CGGGGTACCATGGACTACAAAGACGATG (FLAG-KpnI Forward primer)	CCGCTCGAGTCAGTCTGAGTCAGGCCC
RT-qPCR Primers		
BAX	CTCACTCACCATCTGGAAGAAG	GTGTCCCGAAGGAGGTTTATT
CDKN1A	GAACTTCGACTTTCTCAGCG	TGGAGTGGTAGAAATCTGTC
DRAM1	CGATGGAGTTTCATGCTTCATTT	CACTCTGTTCATTGTGGCATTAC
CDK1	AACTTGGATGAAAATGGCTTGG	AAGAGTTAACAATAAAAACACAACTATCTG
CCNA2	CGAAAGACTGGATATACCCTGG	CATCTTAGAAAACAAAGGCAGTCT
CCNB2	GGCTGGTACAAGTCCACTCC	GAAGCCAAGAGCAGAGCAGT
EP300	AGGCCTATCAGCAGCGACTCCTTCA	TGGGGAGAGCGCACTTGATTGGA

	GC	GAGAG
GAPDH	TCCACCTTTGACGCTGGGGCTGGC	TGGCAGGGACTCCCCAGCAGTGAG
JADE1	CCTAGCTTGGTGTCCATTCA	GGGTAGAAATAAATACAGGATTGGG
ACTB	AGATGTGGATCAGCAAGCAGGAGT	TCCTCGGCCACATTGTGAACTTTG
ChIP-qPCR Primers		
CDKN1A	CAAAATAGCCACCAGCCTCTTCT	AGCAGGCTGGCTCTGATT
BAX	CTCTCGGACCCTCGAGAAC	CTCCCACCAGTGCCAGA
DRAM1	GCCGAGTGTCCAAACCA	CGAAACGAGTGAAGTCACAAAG
GAPDH	TACTAGCGGTTTTACGGGCG	TCGAACAGGAGGAGCAGAGAGCGA
SDM Primers		
L344A p53	CGAGATGTTCCGAGAGGCGAATGAGGCCTTGG	CCAAGGCCTCATTCGCCTCTCGGAACATCTCG
G334V p53	CACCCTTCAGATCCGTGTGCGTGAGCGCTTCGAG	CTCGAAGCGCTCACGCACACGGATCTGAAGGGTG
R337H p53	GATCCGTGGGCGTGAGCACTTCGAGATGTTCCGAG	CTCGGAACATCTCGAAGTGCTCACGCCCACGGATC
R249S p53	GGGCGGCATGAACCGGAGCCCCATCCTCACCATC	GATGGTGAGGATGGGGCTCCGGTTCATGCCGCCC
V143A p53	GCCAAGACCTGCCCTGCGCAGCTGTGGGTTGATTC	GAATCAACCCACAGCTGCGCAGGGCAGGTCTTGGC
R273H p53	GGAACAGCTTTGAGGTGCATGTTTGTGCCTGTCCTGGG	CCCAGGACAGGCACAAACATGCACCTCAAAGCTGTTCC
L194F p53	GCCCCTCCTCAGCATTTTATCCGAGTGGAAG	CCTCCGGTTCATGCTGCCCATGCAGGAAC
R248W p53	GCATGGGCGGCATGAACTGGCGCCCCATCCTCACCATC	GATGGTGAGGATGGGGCGCCAGTTCATGCCGCCCATGC
R175H p53	GACGGAGGTTGTGAGGCACTGCCCCCACCATGAG	CTCATGGTGGGGGCAGTGCCTCACAACCTCCGTC

Transparent Methods

Antibodies

Primary antibodies used in this study: p300 (N-15), Santa Cruz (Catalog no. sc-584); p300 (C-20), Santa Cruz (Catalog no. sc-585); p53 (DO-1), Merck Millipore (Catalog no. OP43); alpha-tubulin (DM1A), Merck Millipore (Catalog no. 05-829). Rabbit polyclonal antibodies against autoacetylated p300 (K1499ac p300), H3K9ac, H3K14ac, H2AK5ac, H3 and GAPDH were raised in-house. Secondary antibodies: Goat Anti-Mouse IgG H&L (HRP), Abcam (Catalog no. ab97023); Goat Anti-Rabbit IgG H&L (HRP), Abcam (Catalog no. ab97051); Goat anti-Rabbit IgG (H+L) Cross-Adsorbed, Alexa Fluor® 488, Thermo Fisher Scientific (Catalog no. A-11008); Goat anti-Mouse IgG (H+L) Cross-Adsorbed, Alexa Fluor® 633, Thermo Fisher Scientific (Catalog no.A-21052).

Cell Culture

Human non-small cell lung carcinoma H1299 cells (ATCC® CRL-5803™, American Type Culture Collection (ATCC), USA) were cultured in RPMI-1640 media supplemented with 2 mM glutamine, antibiotic solution (100 U/ml penicillin, 0.1 mg streptomycin, 0.25 µg amphotericin (HiMedia, India)) and 10% fetal bovine serum (FBS (Life Technologies India, India)). The pEBTetD p53 H1299 cells were cultured in supplemented RPMI-1640 under 1.2 µg/ml Puromycin antibiotic selection. Human hepatocellular carcinoma HepG2 cells (ATCC® HB-8065™, ATCC, USA) and AW13516 cells, a human cell line derived from the Oral cavity squamous cell carcinoma (a kind gift from Dr. Amit Dutt (ACTREC, Mumbai, India)) were cultured in MEM supplemented with 2 mM glutamine, antibiotic solution (100 U/ml penicillin, 0.1 mg streptomycin, 0.25 µg amphotericin) and 10% fetal bovine serum (FBS). The cells were grown at 37 °C in 5% CO_2. Full length His_6-p300, FLAG-PCAF and His_6-Tip60 were expressed in Sf21 (*Spodoptera frugiperda*) insect cells (Thermo Fisher Scientific, USA). The cells were grown in Graces' Media (Gibco, Thermo Fisher Scientific, USA) containing antibiotic solution (100 U/ml penicillin, 0.1 mg streptomycin, 0.25 µg amphotericin) and 10% FBS.

Cloning of p53 constructs

Wild type p53 construct was cloned into BamHI-HF/HindIII-HF sites in the pFLAG-CMV™-2 Mammalian Expression Vector (Sigma Aldrich, USA).pET22b-FLAG-tagged p53 bacterial expression plasmid was generated as described previously (Banerjee et al., 2004).Missense p53 mutants were generated using Site Directed Mutagenesis (SDM) method (QuikChange II XL Site-Directed Mutagenesis, Agilent Technologies) according to the

manufacturer's protocol. The FLAG-tagged p53 construct was subcloned into the Tet-ON mammalian expression plasmid pEBTetD (a kind gift from Prof. Gründemann, University of Cologne, Germany (Bach et al., 2007)) into KpnI/XhoI sites. The construct was amplified using a forward primer designed against the FLAG-tag containing a KpnI restriction site and a reverse primer specific to the 3' end of p53 with a XhoI restriction site. The primers have been listed in Table S3.

Recombinant Protein expression and Purification

His_6-tagged full length p300, Tip60 and FLAG-tagged PCAF were expressed by transfection of the respective recombinant baculovirus into Sf21 insect ovary cells. The His_6-tagged proteins (His_6-p300 and His_6-Tip60) and FLAG-PCAF were purified as described previously (Kundu et al., 1999; Wallberg et al., 2002).

FLAG-p53 and FLAG-p53 mutants were expressed and purified from BL21(DE3)pLysS*E. coli* strain. The recombinant FLAG-tagged p53 proteins were purified through affinity chromatography using M2-agarose (Sigma Aldrich, USA) binding resin as described previously (Gu and Roeder, 1997).

Small Molecule Inhibitor or Peptide treatment

HepG2 cells were treated with the small molecule inhibitor Nutlin-3a (5 μM or 10 μM) for 24 hours (h). The stabilization of p53 and status of p300 autoacetylation and acetylation of p300-substrates were determined by western blotting analysis and immunofluorescence. For the p53-p300 interfering peptides, HepG2 cells were treated with the indicated concentration of Nutlin-3a for 24 h following which the cells were treated with the peptides for 24 h. Western blotting analysis was performed to study the effects of the peptides on p53-mediated modulation of p300 activity.

RT-qPCR

Tet-inducible p53 expression H1299 cells were treated with doxycycline for 24 h. The cells were harvested in TRIzol™ Reagent (Thermo Fisher Scientific, USA) and RNA was isolated according to the manufacturers' instructions. The purified RNA was treated with DNase I (New England Biolabs) at 37 °C for 20 min to remove any contaminating DNA. The RNA was again purified using Phenol-Chloroform-Isoamylalcohol (24:25:1) followed by ethanol precipitation ($1/10^{th}$ volume 3 M sodium acetate, pH 5.2, and 2.5 volumes of 100% ethanol) at -80 °C overnight. cDNA was prepared using M-MLV Reverse Transcriptase (Sigma Aldrich) and oligo dT_{23} primers (Sigma Aldrich). Real Time PCR was performed using SYBR Green (Sigma Aldrich) and mRNA-specific primers (Table S3).

Co-immunoprecipitation

HepG2 cells were treated with 10 μM p53 phosphomimic peptide (3E peptide) or the scrambled control for 24 h. The cells were then treated with 5 μM Nutlin-3a or the vehicle control (DMSO) for another 24 h. The cells were harvested and lysed in RIPA buffer (150 mM NaCl, 50 mM Tris-Cl, 1% NP40, 1% sodium deoxycholate, 1 mM EDTA, and Protease inhibitors). p53 was immunoprecipitated using the DO1 antibody (Merck Millipore, USA). Western Blotting analysis was performed to determine whether p53 and p300 interaction is disrupted by the p53 phosphomimic peptide.

Transfection

1.5 μg wild type p53 or missense mutant p53 plasmids were transfected in H1299 cells using Lipofectamine® 2000 (Thermo Fisher Scientific, USA) reagent according to the manufacturer's instructions. The cells were harvested after 24 h and processed for either western blotting analysis or immunofluorescence.

Wound Healing Assay

Cells were grown in a 30 mm dish or a 6-well plate. When the cells reach ~90% confluency, a scratch was created with a 10 μl tip held at a 45° angle. The cells were given a media change to remove all the floating cells. The wound was monitored over a period of 24 to 48 h till the wound closed. Images of the progress were taken at regular intervals.

Immunofluorescence

H1299, HepG2, and AW13516 cells were grown on poly-lysine coated cover slips at 37 °C in a 5% CO_2 incubator. The media was removed and the cell layer was washed in PBS to ensure all the media was removed. The cells were fixed in 4% para-formaldehyde for 10 min at room temperature. The cells were washed with PBS to remove the remnant PFA. The cells were then permeabilized in 5% Triton X-100. Cells were washed in PBS to remove the residual TritonX-100. The cells were blocked in blocking solution (5% FBS in PBS) at 37 °C for 45 min. The blocked cells were then incubated in primary antibody at the indicated dilution for 1 h at room temperature on a reciprocal shaker. The cells were washed in washing buffer (1% FBS in PBS). The cells were then incubated in Alexa-fluor conjugated secondary antibody corresponding to the primary antibody used, incubated at room temperature for 1 h. The nucleus was counter-stained with Hoechst 33258 (bis-benzamide (Sigma Aldrich, USA)), for 5 min at room temperature. Excess Hoechst stain was washed off with PBS. The cover slips were mounted in 70% glycerol onto a microscope glass slide. The

stained cells were visualized using Carl Zeiss confocal microscopes LSM 510 META or the LSM 880 with Airyscan.

Acetyltransferase Assays

For the p300, Tip60, and PCAF autoacetylation assay, 20 nM KAT enzyme was incubated in HAT assay buffer (50 mM Tris–HCl, pH 7.5, 1 mM PMSF, 0.1 mM EDTA, and 10% v/v glycerol) and 100 mM sodium butyrate at 30 °C for 30 min with or without the protein factors tested as autoacetylation inducersin the presence of 1 µl of 4.7 Ci/mmol [^{3}H]-acetyl-CoA (NEN-PerkinElmer). After the autoacetyltransferase assay, the radiolabeled proteins were processed by fluorography. For the enzyme activity assay, reactions with 1 nM full-length p300 were carried out in HAT assay buffer (50 mM Tris–HCl, pH 7.5, 1 mM PMSF, 0.1 mM EDTA, and 10% v/v glycerol) and 100 mM sodium butyrate at 30 °C for 30 min. The assays were performed with 2 µM histone H3 in the presence of 1 µl of 4.7 Ci/mmol [^{3}H]-acetyl-CoA. After the HAT activity assay, the reaction mix was spotted on p81 phosphocellulose paper, which was washed in wash buffer (0.05 M sodium bicarbonate and 5 mM sodium carbonate). The spotted paper was dried and incubated in scintillation fluid (0.005% PPO and 5x10-4% POPOP in Toluene). The scintillation counts were measured in a scintillation counter (Wallac 1409 Liquid Scintillation Counter, PerkinElmer, USA).

Activity Rescue Assay

The 20 nM p300 was incubated in HAT buffer either at non-denaturating (30 °C, control) or at denaturating conditions (45 °C) for 15 minutes. The denatured enzyme was incubated in the presence of 80 nM and 200 nM p53 at 30 °C for 30 minutes. The substrate (2 µM recombinant histone H3) and [^{3}H] acetyl-CoA were added to the reaction and the reaction was allowed to continue for 15 minutes at 30 °C. The reaction was stopped on ice followed by filter binding assay as described in the earlier section. The activity of p300 at non-denaturing conditions (30 °C) in the absence of NPM1 was considered as 100% activity.

Chromatin Immunoprecipitation

The cells were cross-linked in 1% formaldehyde. The crosslinking was quenched in 0.125 M glycine, the cells were lysed in SDS buffer, and the chromatin was sheared using a Bioruptor® Diagenode (Belgium) instrument. Five to ten micrograms of antibody was used in each ChIP. The antibody and BSA-blocked protein G sepharose beads (GE Healthcare, USA) were added to the cleared sheared cross-linked chromatin and incubated at 4 °C overnight. The beads were then washed to remove non-specific binding with buffers

containing different salt concentrations. The DNA-protein complexes were eluted from the washed beads using a SDS-sodium bicarbonate elution buffer. The eluates and input were de-crosslinked at 65 °C for 6 hours. Proteinase K (Thermo Fisher Scientific, USA) and RNase H (Sigma Aldrich, USA) were added to the de-crosslinked lysates. The DNA was extracted using the phenol:chloroform:isoamyl alcohol method, followed by ethanol precipitation ($1/10^{th}$ volume 3 M sodium acetate, pH 5.2, 20 mg glycogen, and 2.5 volumes of 100% ethanol) at -20 °C overnight.The DNA pellet was washed in 70% ethanol and dissolved in nuclease-free water. ChIP-qPCR was performed using SYBR Green (Sigma Aldrich, USA) and loci-specific ChIP primers (See Table S3).

ChIP-seq and bioinfomatic analysis

The Tet-ON p53 expression cell line was validated through RT-qPCR for the expression of p53-responsive and non-responsive genes upon doxycycline treatment (Figure S2B). Libraries for ChIP-Seq were prepared with KAPA Hyper Prep Kits. The workflow consists of end repair to generate blunt ends, A-tailing, adaptor ligation and PCR amplification. Different adaptors were used for multiplexing samples in one lane. Sequencing was performed on Illumina Hiseq3000/4000 for a single-end 150 run. High quality (HQ) reads with Q20 were generated using NGS QC Tool Kit v.2.3.3 (Patel and Jain, 2012). Filtered reads were aligned against *Homo sapiens* Ensembl build GrCh37 allowing 2 mismatches (-n 2) using the alignment tool Bowtie (Langmead et al., 2009). Post alignment processing including SAM to BAM conversion along with sorting and PCR duplicate removal is performed using SAMTOOLS (Li et al., 2009). BAM files of replicates were merged to get merged Input and IP BAM files for acp300 and p300. Peak calling is performed using MACS14 (Feng et al., 2012) using parameters mfold= 3:10 and p-value of 1e-5 (0.00001) (Figure S2C). The p300 and acp300 peaks were visualized using the Integrated Genome Viewer (IGV) tool (Robinson et al., 2011). HOMER tool (Heinz et al., 2010) was used for finding overlapping genes within distance of 100 bp overlap within acp300 and p300 and to find unique genes specific to acp300 and p300. Total number of peaks obtained were annotated using Peak Analyser v1.4 (Salmon-Divon et al., 2010). Bedgraph files from the peak bed file generated using BEDTOOLS sortBed and GenomeCoverageBed commands. Integration of gene expression data from microarray analysis with ChIP-seq gene enrichment data is carried out to check for the binding occupancy and gene regulation. Average profiles and heatmaps were generated showing ChIP signal densities spanning 5 kb upstream and downstream of TSS using ngs.plot.r(Shen et al., 2014).

Publicly available datasets/ Deposited data

The ChIP-seq data for p300 and acp300 is available at NCBI, SRA Accession ID: SRR5831017. The ChIP-seq data for RNA Pol II, H3K27ac, and H3K4me1 were retrieved from Data Bank of Japan (DDBJ), accession number: DRA001860 (http://dbtss.hgc.jp/) (Suzuki et al., 2014). Microarray of inducible p53 H1299 cell line data: GEO: GSE57841 (Jiang et al., 2015).

Statistics

Unpaired Two-tailed Student's t-test has been used for the statistical analysis. The p-values have been indicated in the figures, legends, and methods.

Key Resources Table

Reagent or Resource	Source	Identifier
Antibodies		
p300 (C-20)	Santa Cruz	sc-585
p300 (N-15)	Santa Cruz	sc-584
K1499ac p300	In-house	n/a
p53 (DO-1)	Merck Millipore	OP43
H3K9ac	In-house	n/a
H3K14ac	In-house	n/a
H2AK5ac	In-house	n/a
H3	In-house	n/a
Goat Anti-Mouse IgG H&L (HRP)	Abcam	ab97023
Goat Anti-Rabbit IgG H&L (HRP)	Abcam	ab97051
Goat anti-Rabbit IgG (H+L) Cross-Adsorbed, Alexa Fluor® 488	Thermo Fisher Scientific	A-11008
Goat anti-Mouse IgG (H+L) Cross-Adsorbed, Alexa Fluor® 633	Thermo Fisher Scientific	A-21052
Chemicals, Peptides, and Recombinant Proteins		
SIGMAFAST™ Protease Inhibitor Cocktail Tablets, EDTA-Free	Sigma Aldrich	S8830
Rnase A	Sigma Aldrich	R6513
Proteinase K	Thermo Fisher Scientific	25530015
TRIzol® Reagent	Thermo Fisher Scientific	15596018
Phenol:Chloroform:Isoamyl Alcohol 25:24:1, Saturated with 10mM Tris, pH 8.0, 1 mM EDTA	Sigma Aldrich	P3803
Chloroform – isoamyl alcohol mixture	Sigma Aldrich	25666

Chloroform	Sigma Aldrich	C2432
Bovine Serum Albumin (BSA)	Sigma Aldrich	B6917
KpnI-HF	New England Biolabs	R3142
XhoI	New England Biolabs	R0146
BamHI-HF	New England Biolabs	R3136
HindIII-HF	New England Biolabs	R3104
Sodium butyrate	Sigma Aldrich	B5887
PfuUltra High-Fidelity DNA Polymerase	Agilent	600380
Phusion® Hot Start Flex DNA Polymerase	New England Biolabs	M0535
Imidazole	Sigma Aldrich	I5513
Ampicillin	Sigma Aldrich	A9393
Isopropyl-b-D-thiogalactopyranoside (IPTG)	HiMedia	RM2578
Acetyl Coenzyme A, [Acetyl-3H]-, 50 µCi (1.85MBq)	Perkin Elmer	NET290050UC
P81 Ion Exchange Cellulose Chromatography Paper	Reaction Biology	IEP-01
Acetyl coenzyme A sodium salt	Sigma Aldrich	A2056
Puromycindihydrochloride	Sigma Aldrich	P8833
Lipofectamine® 2000 Transfection Reagent	Thermo Fisher Scientific	11668019
Glycogen, molecular biology grade	Thermo Fisher Scientific	R0561
Graces Insect Media	Thermo Fisher Scientific	11605102
Minimal Essential Media	Thermo Fisher Scientific	10370021
RPMI-1640 Media	Thermo Fisher Scientific	21870092
Gluta-XL	HiMedia	TCL030
Antibiotic Antimycotic Solution 100X	HiMedia	A002A
Ni-NTA His•Bind® Resin	Merck Millipore	70666
FLAG M2 Agarose	Sigma Aldrich	A2220
Protein G Sepharose 4 Fast Flow	GE Healthcare	17061801
p53(1-39)S15E/T18E/S20E+hexa D-Arg+NLS peptide	In-house	n/a
scrambled+hexaD-Arg+NLS peptide	In-house	n/a
Nutlin-3a	Sigma Aldrich	SML0580
Commercial Assays		
Quant-iT™ PicoGreen ® Assay	Thermo Fisher Scientific	P7589
GeneJET Plasmid Miniprep Kit	Thermo Fisher Scientific	K0502
GeneElute™ Gel Extraction Kit	Sigma Aldrich	NA1111-1KT

KAPA SYBR FAST qPCR Master Mix (2X) Universal	Sigma Aldrich	KK4601
QuikChange II XLSite-Directed Mutagenesis	Agilent Technologies	200522
Softwares and Algorithms		
NGS QC ToolKit V2.3.3	Patel and Jain, 2012	http://www.nipgr.res.in/ngsqctoolkit.html
BOWTIE v1.1.1	Langmead et al., 2009	https://sourceforge.net/projects/bowtie-bio/files/bowtie/
MACS14	Feng J.et al,2011	http://liulab.dfci.harvard.edu/MACS/Download.html
SAMTOOLS	Li H et al., 2009	http://samtools.sourceforge.net/
HOMER	Heinz S et al., 2010	http://homer.ucsd.edu/homer/ngs/index.html
PeakAnalyzer v1.4	Salmon-Divon M.et al., 2010	http://www.ebi.ac.uk/research/bertone/software
NCBI Genome Decoration Page	https://www.ncbi.nlm.nih.gov/genome/tools/gdp/	https://www.ncbi.nlm.nih.gov/genome/tools/gdp
ngs.plot.r	Shen L et al., 2014	https://github.com/shenlab-sinai/ngsplot
bedtools v2.17	Quinlan and Hall., 2010	http://bedtools.readthedocs.io/en/latest/content/installation.html
Integrated Genome Visualization (IGV) tool	Robinson et al., 2012	http://software.broadinstitute.org/software/igv/
MicroArray Analysis	GeneSpring v13.1.1	http://www.genomics.agilent.com/article.jsp?pageId=2192
Deposited Data		
acp300 ChIP-seq	This paper	SRA: SRR5831017; BioProject ID:PRJNA394650 BioSample ID: SAMN07357096
p300 ChIP-seq	This paper	SRA: SRR5831017; BioProject ID:PRJNA394650 BioSample ID: SAMN07357096
RNA POL II ChIP-seq	Suzuki et al., 2014	DDBJ: DRA001860
H3K27ac ChIP-seq	Suzuki et al., 2014	DDBJ :DRA001860
H3K4me1 ChIP-seq	Suzuki et al., 2014	DDBJ: DRA001860
Gene expression microarray from Dox-inducible p53 H1299 cells	Jiang et al, 2015	GEO: GSE57841
Experimental Models: Cell Lines		
H1299	ATCC	ATCC® CRL-5803™
pEBTetD p53 H1299	This study	n/a
pEBTetD R273H p53 H1299	This study	n/a
HepG2	ATCC	ATCC® HB-8065™
AW13516	Dr. Amit Dutt, ACTREC	n/a
Experimental Models: Organisms/Strains		
BL21(DE3)(plysS) *E.Coli*	New England Biolabs	C3010

XL1-BLUE super-competent cells	Agilent	200236
Recombinant DNA		
pFLAG-CMV™-2	Sigma Aldrich	E7033
pFLAG-CMV™-2 p53	This study	n/a
pFLAG-CMV™-2 R273H p53	This study	n/a
pFLAG-CMV™-2 L194F p53	This study	n/a
pFLAG-CMV™-2 R249S p53	This study	n/a
pFLAG-CMV™-2 V143A p53	This study	n/a
pFLAG-CMV™-2 L344A p53	This study	n/a
pFLAG-CMV™-2 G334V p53	This study	n/a
pFLAG-CMV™-2 R337H p53	This study	n/a
pET22b-FLAG-p53	Banerjee et al., 2004	n/a
pET22b-FLAG-T18E p53	Banerjee et al., 2012	n/a
pET22b-FLAG-L344A p53	This study	n/a
pET22b-FLAG-V143A p53	This study	n/a
pET22b-FLAG-R175H p53	This study	n/a
pET22b-FLAG-R248W p53	This study	n/a
pET22b-FLAG-R249S p53	This study	n/a
pET22b-FLAG-R273H p53	This study	n/a
pEBTetD SLC22A1	Bach et al., 2007	n/a
pEBTetD p53	This study	n/a

References

Bach, M., Grigat, S., Pawlik, B., Fork, C., Utermöhlen, O., Pal, S., Banczyk, D., Lazar, A., Schömig, E., and Gründemann, D. (2007). Fast set-up of doxycycline-inducible protein expression in human cell lines with a single plasmid based on Epstein-Barr virus replication and the simple tetracycline repressor. FEBS J. *274*, 783–790.

Banerjee, S., Kumar, B.R.P., and Kundu, T.K. (2004). General transcriptional coactivator PC4 activates p53 function. Mol. Cell. Biol. *24*, 2052–2062.

Feng, J., Liu, T., Qin, B., Zhang, Y., and Liu, X.S. (2012). Identifying ChIP-seq enrichment using MACS. Nat. Protoc. *7*, 1728–1740.

Gu, W., and Roeder, R.G. (1997). Activation of p53 sequence-specific DNA binding by acetylation of the p53 C-terminal domain. Cell *90*, 595–606.

Heinz, S., Benner, C., Spann, N., Bertolino, E., Lin, Y.C., Laslo, P., Cheng, J.X., Murre, C., Singh, H., and Glass, C.K. (2010). Simple combinations of lineage-determining transcription factors prime cis-regulatory elements required for macrophage and B cell identities. Mol. Cell *38*, 576–589.

Jiang, L., Kon, N., Li, T., Wang, S.-J., Su, T., Hibshoosh, H., Baer, R., and Gu, W. (2015). Ferroptosis as a p53-mediated activity during tumour suppression. Nature *520*, 57–62.

Kundu, T.K., Wang, Z., and Roeder, R.G. (1999). Human TFIIIC relieves chromatin-mediated repression of RNA polymerase III transcription and contains an intrinsic histone

acetyltransferase activity. Mol. Cell. Biol. *19*, 1605–1615.

Langmead, B., Trapnell, C., Pop, M., and Salzberg, S.L. (2009). Ultrafast and memory-efficient alignment of short DNA sequences to the human genome. Genome Biol. *10*, R25.

Li, H., Handsaker, B., Wysoker, A., Fennell, T., Ruan, J., Homer, N., Marth, G., Abecasis, G., Durbin, R., and 1000 Genome Project Data Processing Subgroup (2009). The Sequence Alignment/Map format and SAMtools. Bioinformatics *25*, 2078–2079.

Patel, R.K., and Jain, M. (2012). NGS QC Toolkit: a toolkit for quality control of next generation sequencing data. PLoS One *7*, e30619.

Robinson, J.T., Thorvaldsdóttir, H., Winckler, W., Guttman, M., Lander, E.S., Getz, G., and Mesirov, J.P. (2011). Integrative genomics viewer. Nat. Biotechnol. *29*, 24–26.

Salmon-Divon, M., Dvinge, H., Tammoja, K., and Bertone, P. (2010). PeakAnalyzer: Genome-wide annotation of chromatin binding and modification loci. BMC Bioinformatics *11*, 415.

Shen, L., Shao, N., Liu, X., and Nestler, E. (2014). ngs.plot: Quick mining and visualization of next-generation sequencing data by integrating genomic databases. BMC Genomics *15*, 284.

Suzuki, A., Makinoshima, H., Wakaguri, H., Esumi, H., Sugano, S., Kohno, T., Tsuchihara, K., and Suzuki, Y. (2014). Aberrant transcriptional regulations in cancers: genome, transcriptome and epigenome analysis of lung adenocarcinoma cell lines. Nucleic Acids Res. *42*, 13557–13572.

Wallberg, A.E., Pedersen, K., Lendahl, U., and Roeder, R.G. (2002). p300 and PCAF act cooperatively to mediate transcriptional activation from chromatin templates by notch intracellular domains in vitro. Mol. Cell. Biol. *22*, 7812–7819.